

# Towards small and accurate convolutional neural networks for acoustic biodiversity monitoring

Serge Zaugg<sup>1</sup>, Mike van der Schaar<sup>1</sup>, Florence Erbs<sup>1</sup>, Antonio Sanchez<sup>1</sup>,  
Joan V. Castell<sup>1</sup>, Emiliano Ramallo<sup>2</sup>, and Michel André<sup>1\*</sup>

<sup>1</sup>Laboratory of Applied Bioacoustics - Universitat Politècnica de  
Catalunya, Barcelona, Spain

<sup>2</sup>Instituto de Desenvolvimento Sustentável Mamirauá, Tefé, AM, Brazil

\*Corresponding author: michel.andre@upc.edu

December 7, 2023

## Abstract

Automated classification of animal sounds is a prerequisite for large-scale monitoring of biodiversity. Convolutional Neural Networks (CNNs) are among the most promising algorithms but they are slow, often achieve poor classification in the field and typically require large training data sets. Our objective was to design CNNs that are fast at inference time and achieve good classification performance while learning from moderate-sized data. Recordings from a rainforest ecosystem were used. Start and end-point of sounds from 20 bird species were manually annotated. Spectrograms from 10 second segments were used as CNN input. We designed simple CNNs with a frequency unwrapping layer (SIMP-FU models) such that any output unit was connected to all spectrogram frequencies but only to a sub-region of time, the Receptive Field (RF). Our models allowed experimentation with different RF durations. Models either used the time-indexed labels that encode start and end-point of sounds or simpler segment-level labels. Models learning from time-indexed labels performed considerably better than their segment-level counterparts. Best classification performances was achieved for models with intermediate RF duration of 1.5 seconds. The best SIMP-FU models achieved AUCs over 0.95 in 18 of 20 classes on the test set. On compact low-cost hardware the best SIMP-FU models evaluated up to seven times faster than real-time data acquisition. RF duration was a major driver of classification performance. The optimum of 1.5 s was in the same range as the duration of the sounds. Our models achieved good classification performance while learning from moderate-sized training data. This is explained by the usage of time-indexed labels during training and adequately sized RF. Results confirm the feasibility of deploying small CNNs with good classification performance on compact low-cost devices.

# Contents

<b>1</b>	<b>Keywords</b>	<b>3</b>
<b>2</b>	<b>Introduction</b>	<b>3</b>
<b>3</b>	<b>Data and labeling</b>	<b>4</b>
3.1	Data sources . . . . .	4
3.2	Data labeling . . . . .	4
3.3	Data pre-processing . . . . .	5
<b>4</b>	<b>Methods</b>	<b>5</b>
4.1	Receptive field . . . . .	5
4.2	Simple Frequency Unwrapping CNNs . . . . .	6
4.3	Experiments with SIMP-FU CNNs . . . . .	7
4.4	Experiments with image CNNs . . . . .	7
4.5	Training procedure . . . . .	7
4.6	Metric of classification performance . . . . .	8
4.7	Assessment of inference speed . . . . .	8
<b>5</b>	<b>Results</b>	<b>9</b>
5.1	Impact of receptive field . . . . .	9
5.2	Absolute classification performance . . . . .	9
5.3	Inference speed . . . . .	9
<b>6</b>	<b>Discussion</b>	<b>9</b>
6.1	Segment-level vs time-indexed labels . . . . .	9
6.2	Receptive field . . . . .	10
6.3	Model complexity vs performance . . . . .	10
6.4	Inference speed . . . . .	10
6.5	Side note . . . . .	11
6.6	Lookout . . . . .	11
<b>7</b>	<b>Conclusion</b>	<b>11</b>
<b>8</b>	<b>Acknowledgements</b>	<b>11</b>
<b>9</b>	<b>Tables</b>	<b>13</b>
<b>10</b>	<b>Figures</b>	<b>15</b>
<b>11</b>	<b>References</b>	<b>24</b>
<b>12</b>	<b>Appendix</b>	<b>26</b>

# 1 Keywords

Bio-acoustics, Biodiversity, Ecological monitoring, Machine learning, Deep learning, Sensors

## 2 Introduction

Animal species from diverse groups such as birds, mammals, frogs, fishes, and insects produce sounds. The automated and continuous detection of multiple species at multiple sites would be a valuable asset for the monitoring of large-scale changes in biodiversity [1]. The present work is part of a larger project ([www.projectprovidence.org](http://www.projectprovidence.org)) which proposes to implement long-term and large-scale acoustic monitoring of Amazon ecosystems. At project start, labeled reference data for training and testing of supervised classification processes was not available, which is likely to be the case for many bioacoustic projects. Considering the high burden imposed by labeling, we proposed to use moderate-sized training data.

Acoustic monitoring in remote areas like the Amazon forest is challenging. The periodic manual retrieval of data storage devices is not practical. Transmission of data over wireless channels is a promising solution but due to the limited bandwidth this is only feasible if transmitted data volume is heavily reduced. An efficient way to achieve data reduction is to transmit only predictions obtained locally on devices with limited computational capacity. To address this, we evaluated multiple Convolutional Neural Networks (CNNs) to find models that are both fast at inference time and achieve good predictive performance.

CNNs require considerable quantities of labeled data, both for testing and training. Accurate labeling of the test data is critical for a good estimate of predictive performance while accurate labeling of training data generally leads to better models. However, for many species no labeled acoustic data exists. In many monitoring projects, data will have to be labeled from scratch. The ability to work with moderate-sized datasets would be a major asset for such studies.

The labels used in this study mark the start and end of a target sound and are encoded such that this information can be used during network training (See Figure 1). They are called time-indexed labels hereafter. CNNs are prone to "Shortcut learning" and consequently they tend to perform poorly on independent test data [2]. In our setting "Shortcut learning" could occur if patterns from sounds in the close vicinity of the target are used for learning instead of the target sound itself. This risk is reduced by explicitly defining the start and stop time of the targets.

Compared to photograph images, spectrogram patterns are less complex (blurry, one channel, fixed time scale, fixed frequency location). A key assumption of this study was that CNNs with only a few convolutional layers have sufficient expressive power to capture these patterns. In acoustic monitoring the difficulty often arises from the diversity of background noise and presence of other interfering sounds. Simpler CNNs tend to be less prone to over-fitting and under-specification [3]. Over-fitting is especially critical when small training sets have to be used and under-specification could be critical in the presence of correlated interfering sounds. Simpler models are expected to be more robust when deployed in the real-world.

Until recently, research on bioacoustic signal classification has focused on developing feature extraction procedures specifically for a particular problem followed by conven-

tional supervised classification methods. Reviews are available in [4, 5, 6, 7, 1, 8]. Bioacoustic signals are very variable depending on the targeted animals and environments. Generally, feature extraction procedures developed for a particular problem cannot be transferred to other problems. In recent years, Deep Neural Networks (DNNs) have been used successfully for bioacoustic classification tasks, mostly for birds but also other animal groups [9]. DNNs are generally considered superior in terms of classification performance [10] and do not require the tedious development of feature extraction procedure. The majority of bioacoustic studies used CNNs with 2D convolutional filters [11, 12, 13, 14, 15, 16, 17, 18] and a few used recurrent neural networks [19, 20]. In most studies, the acoustic signal was transformed to 2D arrays via the Short Time Fourier Transform (STFT). The log-transformed frequency dimension (Mel-spectrogram) was typically used as input to the DNNs. While many studies used large imaging CNNs, some studies achieved good performance with smaller CNNs consisting of 2-9 convolutional layers [11, 12, 17, 18].

## 3 Data and labeling

### 3.1 Data sources

Acoustic data from the Mamirauá Sustainable Development Reserve (MSDR) in Amazonas, Brazil were recorded with Wildlife SM4 recorders in two periods and stored as one-channel wave files. During Period 1 (July 2016 to April 2017) data were recorded continuously (30 min wave file every 30 min) in 4 sessions of between 3 and 9 days. One minute was randomly extracted from each 30 min file to be manually annotated. This data was used as test set. During Period 2 (August to October 2017) data were recorded with a regular duty cycle (5 min wave files every hour). One minute was randomly extracted from each 5 min file to be manually annotated. This data was used as training set. The randomly extracted data from both periods cover all hours of day and night and they are representative of soundscapes expected in the MSDR. Due to very low counts of some target sounds in the training set, additional data of the 20 bird species were downloaded from the xeno-canto repository ([www.xeno-canto.org](http://www.xeno-canto.org), download criteria see Supplement). These are recordings performed or selected by humans, sometimes with directional microphones. The sounds typically exhibit a high SNR compared to continuous recordings from the wild. They were included in the training data.

### 3.2 Data labeling

A sound-type is defined here as an animal vocalization that can be consistently recognized by human experts and characterized with a few examples. Most bird species produce multiple sound-types which are acoustically distinctive and have a specific behavioral function (e.g. territorial song, contact call, alarm call). Sound-types from 20 bird species that were identified as relevant for bio-acoustic monitoring in the MSDR were searched and labeled for this study (Table 1 and Appendix for details). The start/end point of each sound were marked with bounding boxes with a dedicated labeling tool that allowed in-depth visual and acoustic scrutiny of the sounds. The boxes also included lower and upper frequency bounds but they were not used in this study. The 20 sound-types were assigned to 5 groups according to their typical duration. Twelve sound-types had a fixed duration (Groups FD1, FD2, FD3) and 8 had a variable duration (Groups VD1 and

VD2). The sound-types are summarized in Table 1 and illustrated in Figure 1, and in supplementary Figures 11, 12, 13, 14, 15.

Test data (period 1) were exhaustively searched for the 20 sound-types with the labeling tool. Each single segment was scrutinized even if it contained only background noise and all signals that could be discerned were labeled. Training data (Period 2 and xeno-canto) were labeled with computer aided labeling. Candidate regions were first identified via model-based predictions with a low decision threshold to minimize the number of false negatives. Candidate regions were then manually labeled by a human expert with the dedicated tool.

### 3.3 Data pre-processing

Acoustic data from MSDR were recorded as waveforms (WAV format) with a sampling rate of 48000 samples per second (sps) and data from xeno-canto were downloaded as MP3 and converted to WAV with a sampling rate of 48000 sps. All files were processed by segments of 10 seconds. For the training set this resulted in 10242 segments from Period 2 plus 1099 segments from xeno-canto. For the test set this resulted in 5635 segments from Period 1 (detail in Appendix Table 7). The high sampling rate was motivated by the detection of ultrasonic sounds of some mammals which are not the focus of this study. All bird sounds used here were located in frequencies below 5000 Hz. Frequencies below 100 Hz were dominated by ambient noise (wind, water). Therefore, the operational range of the classifier was set to 100-5000 Hz. The waveforms were pre-processed by segments of 10 seconds in several steps to obtain standardized Mel-spectrograms: (1) compute the Short Time Fourier Transform (STFT, Hann window of 2048 samples = 0.04 s, 54% overlap), (2) select frequency bins between 100 Hz and 5000 Hz, (3) apply absolute value and log to the STFT, (4) equalize STFT by subtracting the per-frequency median, (5) apply 128 Mel-scaled filters to the frequency dimension of the STFT. Mel-scaling emphasizes the resolution of lower relative to higher frequencies. This allows a considerable reduction in array size while conserving information content of the spectrograms. (6) Finally, normalize amplitude to have zero mean and unit standard deviation. The result is a matrix of 512 time bins by 128 frequency bins.

The original annotations were the start/end point of each of the 20 sound-types and as such they cannot be directly used to train CNNs. The annotations were transformed into binary matrices of size 512 by 20 (time by number of classes) that encode the presence of each sound at a particular time. If necessary the time dimension of these matrices was down-sampled via block-wise max pooling to match the size of the CNN’s output. These binary matrices will be referred to as time-indexed labels hereafter. Visual representations of spectrograms and time-indexed labels are shown in Figure 1 and in supplementary Figures 11, 12, 13, 14, 15.

## 4 Methods

### 4.1 Receptive field

The Receptive Field (RF) of a CNN is a region of the input array (in our case a spectrogram) that is connected to one unit of the output array. In other words, how much of the input spectrogram can one output unit ‘see’. Intuitively, if it sees too long regions it might wrongly learn from surrounding background signals. If it sees too short regions, it

will not leverage the full pattern of a sound during the learning process. In this article the focus is on the time dimension where the input has 512 units (10 sec) and the output between 1 and 512 units, depending on the model. For our models we report the Maximum Receptive Field (MRF, Table 4) which can be derived by arithmetic calculation (see for example eq. 2 in [21]). Recent research has defined the Effective Receptive Field and shown that units closer to the center of the receptive field have a larger impact on the output value [22]. Therefore the MRF that we report here should be considered an upper bound on Effective Receptive Field size.

## 4.2 Simple Frequency Unwrapping CNNs

We defined a family of CNNs which take spectrograms as input (time x frequency) and return time-indexed, multi-label outputs (time x class). In this study, all models had a fixed input size (512 x 128) while the output had variable time resolutions ranging from 1 (full pooling) to 512 time bins (no pooling). The number of classes was always 20. Any output unit is connected to all 128 frequency bins of the input spectrogram but only to a local region of its time bins. This region is referred to as the MRF hereafter. This was achieved through a Frequency Unwrapping (FU) layer which is explained below and illustrated with a minimal example in Figure 2. A full description of SIMP-FU models is provided in Figure 3. The MRF over time of an output unit was inversely related to the output time resolution (See Table 4).

These architectures allowed us to manipulate the MRF over time. A specific architecture is called a ‘model’ hereafter. Detailed descriptions of a few models are given in Tables 2 and 3 and a summary of all models in Table 4. All CNNs used batch normalization in the convolutional layers and ReLU as transfer functions, sigmoid transfer was used only in the output layer. To avoid an explosion in number of weights, linear increment in channel depth was used in most experiments (A,B,C,D). All models have 3 main regions (see Figure 3) which are described hereafter.

**Conv2D Region** This region was inspired by the VGG architecture [23]. It is basically a sequence of convolutional blocks with receptive field 5x5 (3x3 and 3x3) followed by 2x2 max-pooling. The number of convolutional blocks varied from 0 to 7 (Tables 2 and 3). In Figure 3 only two blocks are depicted.

**Frequency Unwrapping Region** The output of the last max-pooling layer is reshaped from 3D to 2D by unwrapping the frequency dimensions into the channel dimension, while the time dimension is conserved (Figure 2 and 3 Box b). This has an important impact on the CNN’s overall connectivity: Any output unit is connected to all frequency bins of the input spectrogram but only to a local subset of its time bins.

**Conv1D Region** The output of the Frequency Unwrapping Region was fed into two consecutive 1D convolution layers to allow further nonlinear combination of the channel dimension. These two layers were fixed to 256 channels in all experiments. The convolutional kernel size was fixed to 1 to avoid additional increment of the MRF in time which by design is meant to be controlled only in the Conv2D Region. Finally, the output layer is a 1D convolution (also kernel size = 1) with height equal to the number of time bins and depth equal to number of classes (Figure 3, right). Sigmoid transfer was used in the output layer to implement multi-label classification (multiple classes can be present simultaneously). At training time, binary cross-entropy loss was used.

### 4.3 Experiments with SIMP-FU CNNs

In 5 series of experiments (A to E) we assessed several SIMP-FU architectures. Each series had 8 models covering several values of MRF. See Table 4 for details. **(A)** In a first series (A00-A07) the objective was to modify the MRF in time while keeping the total network depth constant. This was achieved by setting kernel and max-pooling in some layers to 1 along the time dimensions as shown in Table 2. At the one end, model A00 used 7 standard convolutional blocks (5x5) resulting in a large MRF of 636 time bins (12.4 sec). MRF can be larger than the input array because padding was used in the convolutional layers. At the other end, Model A07 used only 1x5 convolutional blocks which do not act on the time dimension and the output has 512 time bins (same as the input) and an MRF size of 1 bin (0.02 second). **(B)** In a second series (B00-B07) we used same MRF values as in the first series while making the models shallower. The 1x5 convolutional blocks were removed (Table 3). The B models have a lower level of nonlinear combinations along the frequency dimension in the Conv2D region. **(C)** In a third series (C00-C07) we assessed the usage of simpler segment-level labels because this would reduce the annotation workload. The models from B were modified by including average pooling over time just before the output (Figure 3, Box C). In this form they return exactly one value per class and per segment. In a way, the task of identifying the relevant time region is handed over from the human labeler to the training procedure.

The models from A,B, and C have linear layer depth increment (32, 64, 96, 128, 160, 192, 224). **(D)** In a fourth series (D00-D07), models were as in B but with depth multiplied by two (64, 128, 192, 256, 320, 384, 448). **(E)** In the fifth series (E00-E07), models were as in B but with exponential increment of depth (32, 64, 128, 256, 512, 1024, 2048). A few models from D and E are equal to models from B and they are marked with an asterisk in Table 4.

### 4.4 Experiments with image CNNs

Two of the smaller CNNs developed for image classification were adapted for our setting (Mobilenet V2 [24, 25], Densenet 121 [26]). These architectures have a pooling factor of 32 at the output of the convolutional blocks. The input 512 x 128 is mapped to an output of 16 x 4. These models natively include global average pooling over the time and frequency dimensions. A first baseline experiment aimed at modifying the models minimally (DEN00, MOB00). The last layer (softmax) was replaced by a sigmoid layer to implement multi-label classification as in the SIMP-FU models. In a second experiment (DEN01, MOB01), the output of their convolutional region was piped into the Frequency Unwrapping and Conv1D blocks of our models (i.e. Conv2D region in Figure 3 was replaced by the Conv2D region of the image CNNs). Thereby the 4 frequency bins were mapped to separate channels in the Conv1D part while the time resolution at the output was 16. These two models are most comparable to SIMP-FU models of type '-02' (Table 4) which also have an output time resolution of 16.

### 4.5 Training procedure

The training data was up-sampled on a per class basis to achieve a higher balance across the 20 classes (Table 1). Training-time data augmentation of the spectrograms was applied with the following random distortions: (1) limited range frequency shift, (2)

time-shift, (3) mixing of any two randomly selected segments from the training set, including labels. Thereby xeno-canto sounds were often mixed with Mamirauá background noise. One epoch was defined as a training cycle over the up-sampled datasets (14670 segments). SIMP-FU models were trained for 11 epochs, and training was replicated 4 times with different random initialization of the weights and random distortion from data augmentation. The Adam optimizer [27] was used with initial learning rate = 0.001 and learning rate decay = 0.001. Binary cross-entropy was used as loss function. A batch size of 32 was used. The same procedure was used for models DEN and MOB but with a batch size of 16 and 18 epochs. When adequate, the binary labels were down-sampled via block-wise max pooling to match the output’s time resolution. CNNs were implemented with TensorFlow 2.7.0 and trained on an GPU (NVIDIA GeForce RTX 2060).

## 4.6 Metric of classification performance

Models returned predictions as a matrix with  $N = 20$  classes and time resolution between 1 and 512 time bins (Figure 3). Test performance was computed at the level of segments. Predictions were summarized as the mean over time for each class to obtain 20 values in  $[0,1]$ . For each of the 20 classes, the Average Precision (AP) and Area Under the ROC Curve (AUC) were obtained with the 5635 test segments. As overall performance metrics, the unweighted mean over the per-class metrics (macro mean) was reported for both AP and AUC. Per-class metrics were also reported separately. In our test set, the abundance was very variable depending on the class (Table 1). AUC is insensitive to differing abundance of the classes while AP is sensitive in a way that frequent sound tend to get higher values. AP values are therefore more difficult to compare across classes. As a reference, a classifier that predicts at random gets  $AUC = 0.5$  and AP equals the relative proportion of calls, a hypothetical perfect classifier gets  $AUC = 1.0$  and  $AP = 1.0$ . These two metrics were chosen because they quantify the ability to separate the classes independently of a particular threshold. Methods to choose a threshold were not addressed because it was not the primary focus of this study.

## 4.7 Assessment of inference speed

In a deployment scenario, data will typically be processed in segments of fixed length. A high level of time coverage can be achieved with consecutive segments but this is also costly in terms of computation. This more costly scenario was assessed here. For real-time processing, inference must be faster than the time elapsed between two segments. Here, faster than 10 seconds. For GPU-powered batch processing of large collections of recorded data, inference should be orders of magnitude faster than total data duration. Inference speed was reported as the processing factor (the segment length divided by its inference time). This metric informs on inference time relative to a segment’s duration; larger value means faster inference. On compact low-cost devices (Raspberry Pi), segments were processed one at a time with a single thread to mimic their sequential acquisition. On GPU-powered machines, inference was performed by batches of 32 segments.

## 5 Results

### 5.1 Impact of receptive field

Models using time-indexed labels (A,B,D,E) performed considerably better than their segment-level counterparts (C). Within the group of time-indexed models, the primary driver of performance was the MRF size. Highest overall performances were achieved at intermediate MRF values of 76 time bins (1.48 sec). There was a drop in performance as MRF became larger or smaller. See Figures 4 and 5. The performance of models in groups A and B was almost equal except for the two smallest MRF values of 1 and 6. Models with deeper convolutional blocks (D,E) performed better than the shallower models from groups B. Noticeably, on a per-class basis, the same association between MRF and classification performance was observed in the majority of classes (Figures 6 and 7). FU-modified image CNNs (DEN01, MOB01) performed better than their respective unmodified counterparts (DEN00, MOB00). DEN01 performed best among image CNNs but lower than the best SIMP-FU models (Figure 8).

### 5.2 Absolute classification performance

In absolute terms, classification performance of some SIMP-FU models was good, e.g. Model E03 with AUC above 0.95 in 18 sound-types and even above 0.98 in 13 sound-types (Figure 9 a). Out of 12 sound-types with abundance below 0.01, 10 reached AP above 0.5. Out of 8 other sound-types with abundance below 0.10, 6 reached AP above 0.5 (Figure 9 b).

### 5.3 Inference speed

On compact low-cost hardware (Raspberry Pi) using only one thread, D03 evaluated approx. two times faster than data acquisition, E03 five times, and B03 seven times faster (Figure 10 a). In terms of speed, MOB01 was the fastest and DEN01 was in the same range as E03. However, the classification performance of MOB01 and DEN01 was lower than the SIMP-FU models. On GPU D03 evaluated approx. 3000 times faster than data acquisition while B03 and E03 evaluated approx. 6000 times faster (Figure 10 b).

## 6 Discussion

### 6.1 Segment-level vs time-indexed labels

In the current setting of moderate number of training examples, time-indexed models were superior to segment-level models (Groups A,B,D,E vs. C in Figures 4 and 5). The better generalization performance of time-indexed models can be explained by at least two mechanisms: (1) Many sound-types are shorter than the segments and time-indexed labeling explicitly marks the surrounding noise as background such that the time-indexed models can learn to discriminate the target sound from its direct surrounding. This reduces the risk of wrongly learning background patterns that co-occurred with target sounds in the training set. (2) In data augmentation, the mixing of 2 segments with time-indexed labels allowed to create diverse situations where two different sound-types were in the same segment but generally only partially overlapped. It thereby increased

the diversity of the training set by creating challenging situations that were infrequent in the un-augmented data. Time-indexed annotation with bounding boxes was more work intensive than just tagging the presence of sounds at the level of segments. Our results show that time-indexed annotation was worth the effort.

## 6.2 Receptive field

The best performing MRF of 1.48 seconds is in the same range as the duration of 8 fixed duration sounds (FD2, FD3) but shorter than 4 sounds (FD1) (Table 1). For all 8 variable duration (VD) sounds an MRF of 1.48 seconds seems sufficient to capture a few basic units of the repeating pattern (see figures in Appendix). In summary, the MRF of 1.48 is adequate to capture the full informative patterns of 16 sounds but it can only capture partial information in 4 sounds of the group FD1. Due to the segmented nature of the data, training examples of longer sounds (FD1) were often truncated and due to overlap with other sounds they were often partially masked. Hence, many training examples of FD1 were de-facto shorter than the full duration of the sounds. This may have prevented the CNNs from learning longer patterns. Working with longer segments, e.g. one minute, should be assessed in the future. A key lesson from our study is that the duration of the receptive field matters.

Our models taken individually impose a single MRF on all 20 sound-types. In our dataset short sounds or repetitive sounds with a short base pattern were predominant and pointed us to relatively short value of MRF. The current study design probably prevented us from finding optimal models for the longer sounds. In the future we propose to train separate models for shorter and longer sounds or even dedicated models for each class.

## 6.3 Model complexity vs performance

Within each depth group, the best performing models were D03, E03, and B03 with 2.4, 1.7 and 0.7 millions trainable weights. These three models were smaller and achieved better classification performance on an acoustic classification task compared to the best image CNN, DEN01, with 8.1 M weights. Generally, the patterns found in spectrogram data are considerably simpler than patterns in photograph images. The expressive power of SIMP-FU models seems sufficient to handle the complexity of acoustic patterns from the 20 sound-types considered here. Many animal sounds are expected to fall into this category of complexity. We propose that under the constraint of moderate-sized training sets, simple CNNs such as SIMP-FU models can be used for bioacoustic monitoring.

## 6.4 Inference speed

While model D03 performed best in terms of predictive performance, it was only two times faster than acquisition rate on low-cost hardware. Considering that other processes need to run on deployed sensors (e.g. spectrogram computation, equalization and normalization), this is probably too slow. Models B03 and E03 were close in predictive performance and evaluated 5 and 7 times faster, which leaves sufficient resources for other processes. Model E03 seems to offer a good balance between speed and classification performance; it has 32 channels in the first layers vs 64 for model D03. This considerable improvement in speed is because early convolutional layers are the most time consuming as they act on the 'full-sized' spectrogram. To further optimize the trade-off between

speed and classification performance, future research should also focus on the first layer and on minimizing the size of the spectrogram.

GPUs can be used for batch processing of large data collections. On GPU the faster well performing models (B03 and E03) ran twice as fast as the larger model (D03). This is a considerable difference, especially considering that access to GPU powered machine is limited in institutions with low financial resources. E03 seems to offer an optimal balance between speed and predictive performance also on GPU.

## 6.5 Side note

A full data processing pipeline for long-term bioacoustic monitoring must include more steps that were not addressed here, such as: (1) smart choice of decision thresholds based on expected call rate, (2) handling of interference sounds such as heavy rain/wind, plane and ship engine, human speech, saturation due to the animal very close to microphone, (3) aggregated decision values at periods longer than 10 seconds, e.g. 5 minutes.

## 6.6 Lookout

Large scale bioacoustic monitoring will need to include many animal species from diverse groups. However, only moderate or even small datasets can be expected to be available for training in general because labeling is a fundamental bottleneck in ML projects. Our models achieved good predictive performance by learning from a moderate-sized training set with less than 100 examples in most classes. Such small models could be an important contribution to realize large scale bioacoustic monitoring. Complementary to large data-greedy DNNs that handle all classes at once, we envision ensembles of smaller CNNs with well defined properties like the MRF, where each CNN is adapted for a particular groups of sounds. We used a single input frequency range for all classes (100-5000 Hz). In the future it could be advantageous to use dedicated CNNs for several smaller frequency ranges.

## 7 Conclusion

1. The duration of the receptive field was identified as a critical aspect that conditions the generalization performance of CNNs used for bioacoustic classification.
2. Models that can leverage time-indexed labels during training achieved considerably better generalization performance compared to models that use labels at the level of 10 seconds.
3. For bioacoustic classification, comparison of models covering a wide range of capacities showed that smaller and faster models had better generalization performance.
4. Our results confirm the feasibility of deploying small CNNs with good generalization performance on a large number of compact low-cost devices.

## 8 Acknowledgements

We would like to thank Guilherme Costa Alvarenga, Kotaro Tanaka, Monika Kosecka, Pedro Nassar, Valciney Martins, and Wezddy Del Toro Orozco for their valuable help in

defining the sound classes and during the early phase of labelling the sound examples. We are very thankful to the Gordon and Betty Moore Foundation ([www.moore.org](http://www.moore.org)) who funded Project PROVIDENCE and helped set the basis for the current work.

## 9 Tables

Species	Short name	Group	Description	Train	Train	Test	Test
— Fixed duration			— Approx duration	N	N ups.	N	Prop
<i>Attila bolivianus</i>	ATT-BOL	FD1	3+ sec	32	224	115	0.02
<i>Taraba major</i>	TAR-MAJ	FD1	3+ sec	40	200	15	0.003
<i>Nyctibius griseus</i>	NYC-GRI	FD1	3+ sec	39	234	10	0.002
<i>Xiphorhynchus guttatus</i>	XIP-GUT	FD1	3+ sec	41	205	40	0.007
<i>Myrmelastes hyperythrus</i>	MYR-HYP	FD2	1 – 3 sec	40	224	33	0.006
<i>Xiphorhynchus obsoletus</i>	XIP-OBS	FD2	1 – 3 sec	33	231	8	0.001
<i>Crypturellus undulatus</i>	CRY-UND	FD2	1 – 3 sec	116	251	96	0.017
<i>Nasica longirostris</i>	NAS-LON	FD3	0.5 – 1 sec	64	297	65	0.012
<i>Nyctibius grandis</i>	NYC-GRA	FD3	0.5 – 1 sec	60	243	22	0.004
<i>Psarocolius angustifrons</i>	PSA-ANG	FD3	0.5 – 1 sec	38	228	24	0.004
<i>Pitangus sulphuratus</i>	PIT-SUL	FD3	0.5 – 1 sec	73	222	26	0.005
<i>Leptotila rufaxila</i>	LEP-RUF	FD3	0.5 – 1 sec	62	269	420	0.075
— Variable duration			— Repet. interval				
<i>Ramphastos tucanus</i>	RAM-TUC	VD1	0.5 sec	94	323	44	0.008
<i>Trogon melanurus</i>	TRO-MEL	VD1	0.7 sec	93	331	38	0.007
<i>Capito aurovirens</i>	CAP-AUR	VD1	0.5 sec	313	449	90	0.016
<i>Glaucidium brasilianum</i>	GLA-BRA	VD1	0.3 sec	87	265	33	0.006
<i>Amazona festiva</i>	AMA-FES	VD2	irregular	99	305	213	0.038
<i>Cacicus cela</i>	CAC-CEL	VD2	irregular	111	229	95	0.017
<i>Crotophaga major</i>	CRO-MAJ	VD2	irregular	27	216	22	0.004
<i>Monasa nigrifrons</i>	MON-NIG	VD2	irregular	135	300	250	0.044
Total nb of segments				11341	14670	5635	

Table 1: Grouping of sound-types according to their typical duration and summary of training and test data. FD: Fixed Duration, VD: Variable duration. N: count of segments containing a particular sound-type. N ups: count after re-balancing classes of training set. The total nb of segments was larger than the sum of counts because many segments did not contain any of the 20 sound-types. Proportion of each sound-type in test set is given in last column.

	A00	(Conv) (mp)	A03	(Conv) (mp)	A07	(Conv) (mp)
input	512 x 128 x 1	(5x5) (2x2)	512 x 128 x 1	(5x5) (2x2)	512 x 128 x 1	(1x5) (1x2)
output block 1	256 x 64 x 32	(5x5) (2x2)	256 x 64 x 32	(5x5) (2x2)	512 x 64 x 32	(1x5) (1x2)
output block 2	128 x 32 x 64	(5x5) (2x2)	128 x 32 x 64	(5x5) (2x2)	512 x 32 x 64	(1x5) (1x2)
output block 3	64 x 16 x 96	(5x5) (2x2)	64 x 16 x 96	(5x5) (2x2)	512 x 16 x 96	(1x5) (1x2)
output block 4	32 x 8 x 128	(5x5) (2x2)	32 x 8 x 128	(1x5) (1x2)	512 x 8 x 128	(1x5) (1x2)
output block 5	16 x 4 x 160	(5x5) (2x2)	32 x 4 x 160	(1x5) (1x2)	512 x 4 x 160	(1x5) (1x2)
output block 6	8 x 2 x 192	(5x5) (2x2)	32 x 2 x 192	(1x5) (1x2)	512 x 2 x 192	(1x5) (1x2)
output block 7	4 x 1 x 224		32 x 1 x 224		512 x 1 x 224	
freq. unwr.	4 x 224	(1) (na)	32 x 224	(1) (na)	512 x 224	(1) (na)
output conv1D	4 x 256	(1) (na)	32 x 256	(1) (na)	512 x 256	(1) (na)
output conv1D	4 x 256	(1) (na)	32 x 256	(1) (na)	512 x 256	(1) (na)
output T x Cl	4 x 20		32 x 20		512 x 20	
—	—	—	—	—	—	—
MRF (time bins)	636		76		1	
MRF (seconds)	12.42		1.48		0.02	

Table 2: Description of array and convolutional kernel sizes in 3 models from the A group. mp: max pooling, T: Time, F: Frequency, Ch: Channel, Cl: Classes. Before frequency unwrapping array size given as T x F x Ch and after as T x Ch

	B00	(Conv) (mp)	B03	(Conv) (mp)	B07	(Conv) (mp)
input	512 x 128 x 1	(5x5) (2x2)	512 x 128 x 1	(5x5) (2x2)	512 x 128 x 1	
output block 1	256 x 64 x 32	(5x5) (2x2)	256 x 64 x 32	(5x5) (2x2)		
output block 2	128 x 32 x 64	(5x5) (2x2)	128 x 32 x 64	(5x5) (2x2)		
output block 3	64 x 16 x 96	(5x5) (2x2)	64 x 16 x 96	(5x5) (2x2)		
output block 4	32 x 8 x 128	(5x5) (2x2)	32 x 8 x 128			
output block 5	16 x 4 x 160	(5x5) (2x2)				
output block 6	8 x 2 x 192	(5x5) (2x2)				
output block 7	4 x 1 x 224					
freq. unwr.	4 x 224	(1) (na)	32 x 1024	(1) (na)	512 x 128	(1) (na)
output conv1D	4 x 256	(1) (na)	32 x 256	(1) (na)	512 x 256	(1) (na)
output conv1D	4 x 256	(1) (na)	32 x 256	(1) (na)	512 x 256	(1) (na)
output T x Cl	4 x 20		32 x 20		512 x 20	
—	—	—	—	—	—	—
MRF (time bins)	636		76		1	
MRF (seconds)	12.42		1.48		0.02	

Table 3: Description of array and convolutional kernel sizes in 3 models from the B group. Letter-Codes: see Table 2

Model group	Model Number	-00	-01	-02	-03	-04	-05	-06	-07
A	— Nb conv. Blocks	7	7	7	7	7	7	7	7
	32-lin	2457206	1898102	1492598	1216118	1044086	951926	915062	908726
B	— Nb conv. Blocks	7	6	5	4	3	2	1	0
	32-lin	2457206	1658230	1114422	797110	669430	661750 (*2)	606134 (*3)	104980 (*4)
C (*1)	32-lin	2457206	1658230	1114422	797110	669430	661750	606134	104980
D	64-lin	9487062	6211798	3907670	2443606	1672150	1380310	1158486	104980 (*4)
E	32-exp	76105334	19471990	5311094	1769590	883574	661750 (*2)	606134 (*3)	104980 (*4)
—	Time resol. at output (*1)	4	8	16	32	64	128	256	512
—	MRF (time bins)	636	316	156	76	36	16	6	1
—	MRF (seconds)	12.42	6.17	3.05	1.48	0.7	0.31	0.12	0.02

Table 4: Summary of all SIMP-FU models with number of trainable weights (upper part of table). Within each model group there were 8 models (00 to 07) with different output shape and MRF (lower part of table). \*1 Model C as B but with average pooling over time in the layer preceding output. In C, time resolution is value before average pooling. \*2 Model B05 = E05; \*3 B06 = E06; \*4 B07=E07=D07; only B05, B06, and B07 reported in figures. Increment in channel depth: 32-lin: 32, 64, 96, 128, 160, 192, 224. 64-lin: 64, 128, 192, 256, 320, 384, 448. 32-exp: 32, 64, 128, 256, 512, 1024, 2048.

model	based on	Modified	trainable weights
DEN00	Densenet 121	Sigmoid output	6968084
DEN01	Densenet 121	GA repl. by FU	8068372
MOB00	Mobilenet V2	Sigmoid output	2248916
MOB01	Mobilenet V2	GA repl. by FU	3606228

Table 5: Overview of modified image CNNs used in this study. GAP: Global Average Pooling. FU: Frequency Unwrapping

## 10 Figures

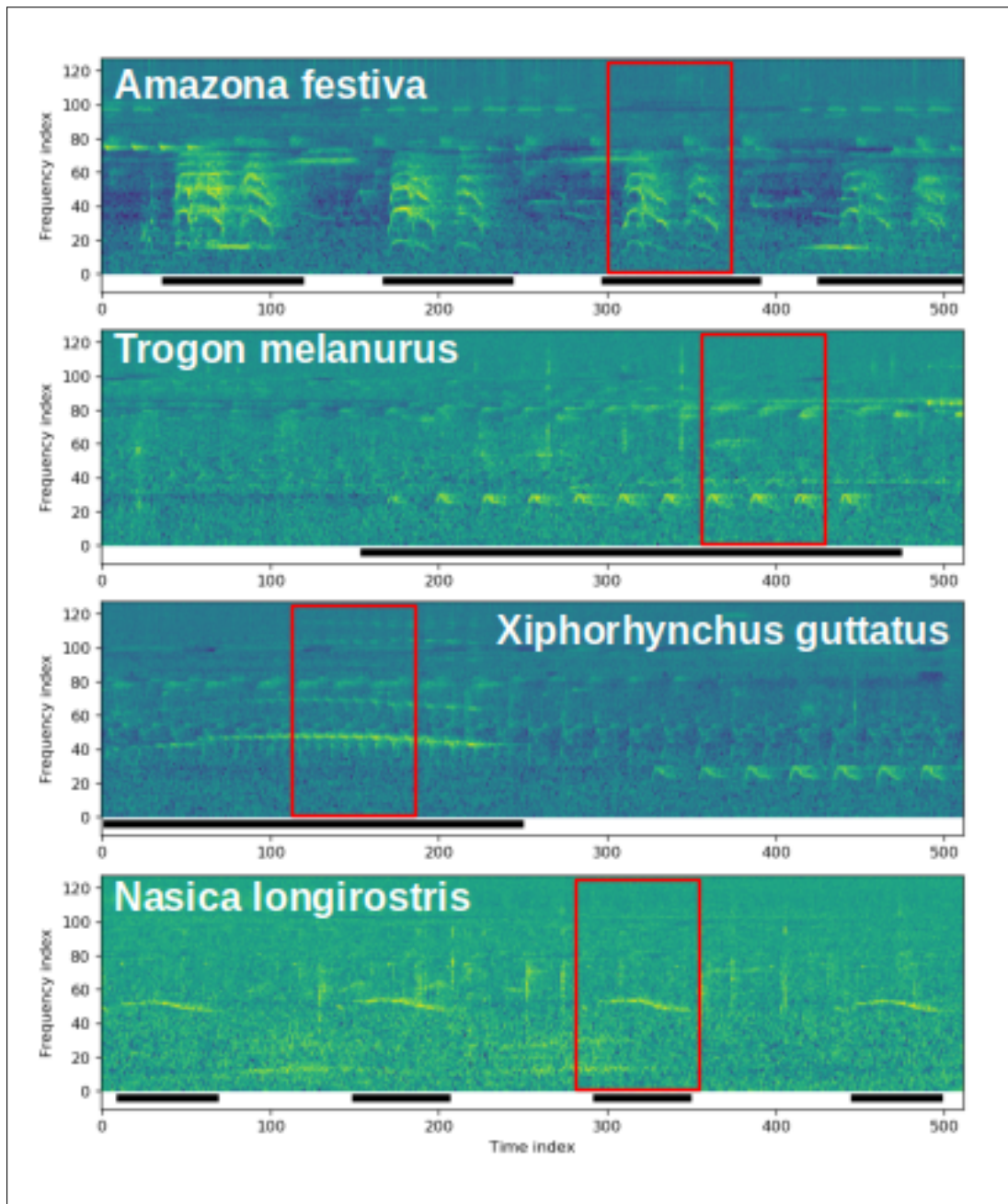


Figure 1: Spectrograms used as CNN input. Four sound-types shown here; all 20 in Supplement. Time-indexed labels used as target during training shown as black bars at the bottom of each spectrogram. Manually selected Regions of 1.5 seconds shown as red boxes to allow visual comparison with the time scale of acoustic patterns.

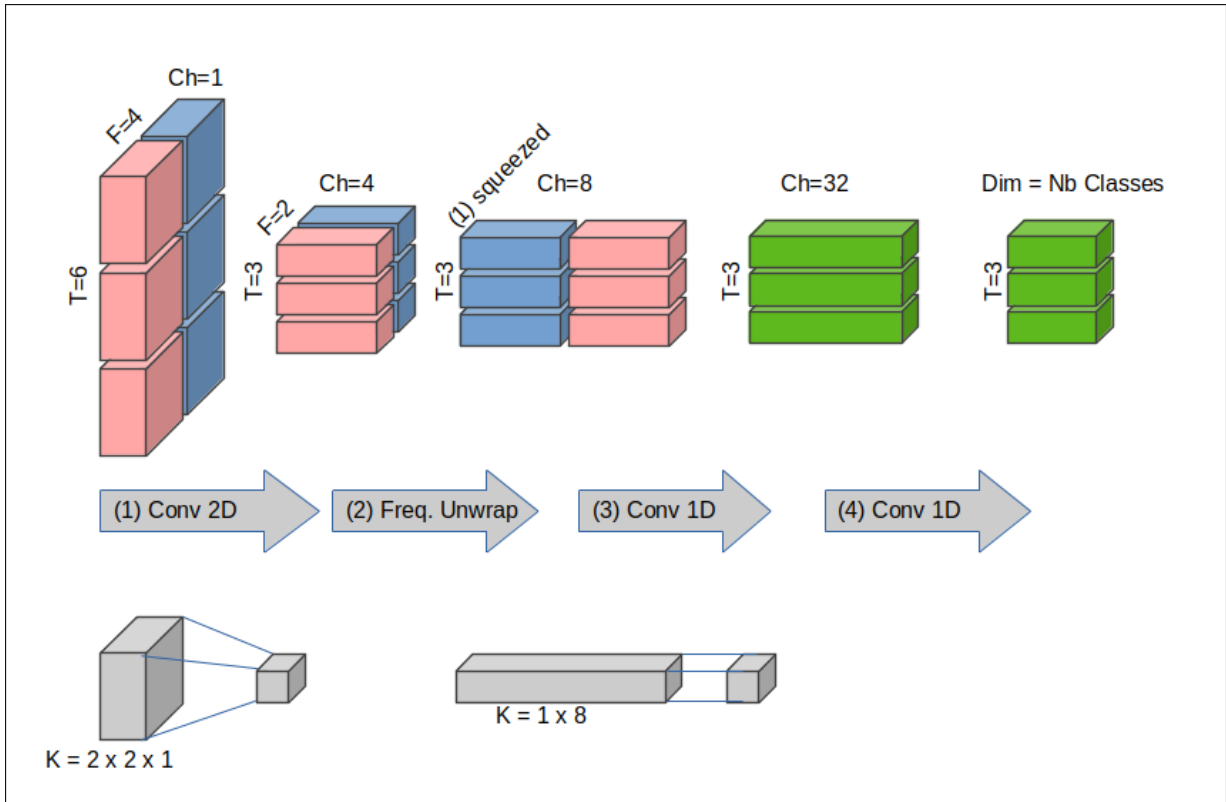


Figure 2: Differential processing of Time (T) and Frequency (F) by SIMP-FU models illustrated with a minimal example. (1) The input array goes through 2D convolution, T and F are down-sampled by 2x2 while Channel (Ch) is increased from 1 to 4. Convolution regions do not overlap here for clarity. (2) Frequency is unwrapped into the Channel dimension. (3) 1D convolution, Nb Ch arbitrarily set to 32. (4) 1D convolution which maps the 32 channels to output (20 classes). The 1D convolutions use kernel size along time = 1, which is equivalent to fully-connected layers with weights shared across time. Any output unit is connected to all frequencies but only to one of the 3 input time-blocks.

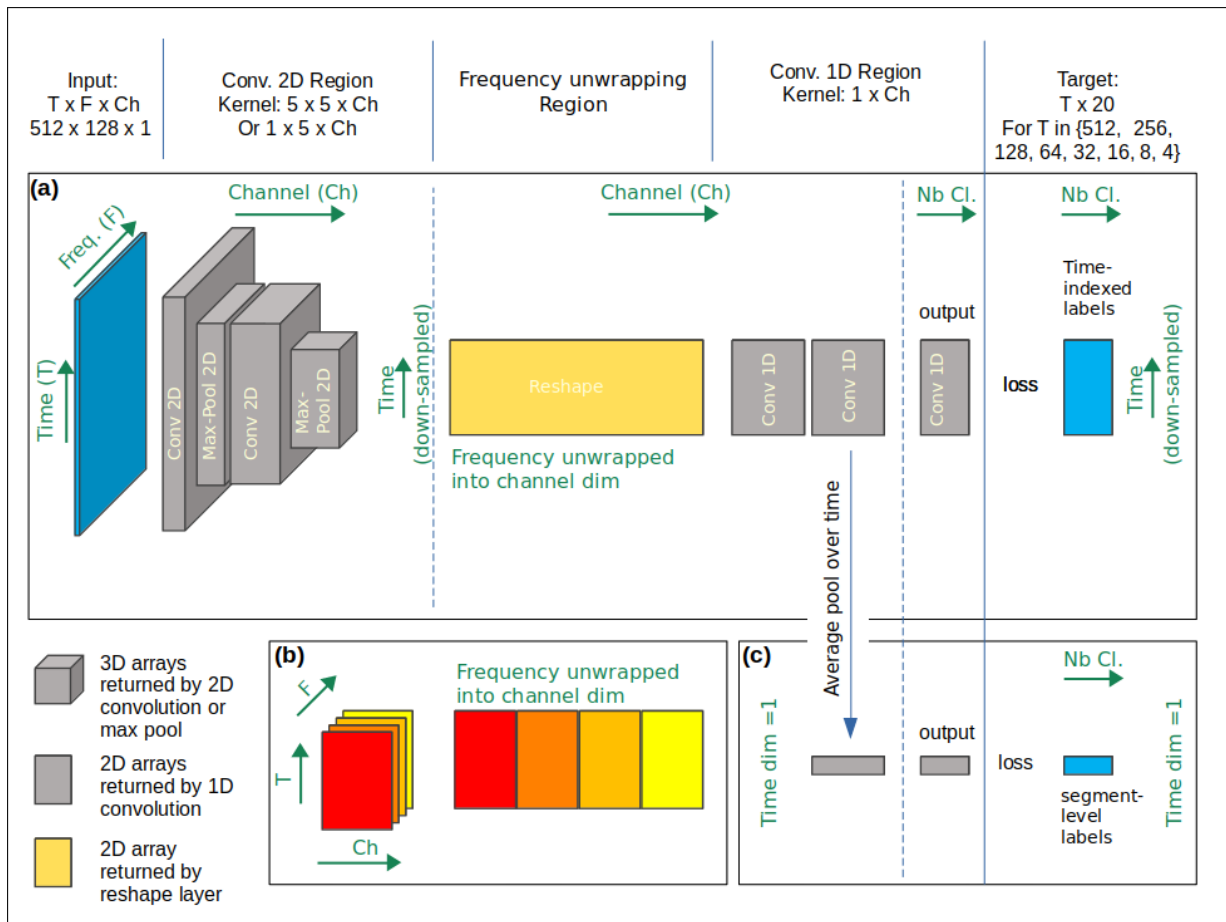


Figure 3: Overview of the SIMP-FU architectures. Only two 2D convolutional blocks shown here, but between 0 and 7 were used in the actual models. (a) Full schematics of a SIMP-FU CNN with time-indexed labels. (b) Illustration of frequency unwrapping. (c) Alternative output for segment-level labels. Grey blocks represent the output arrays of the layers

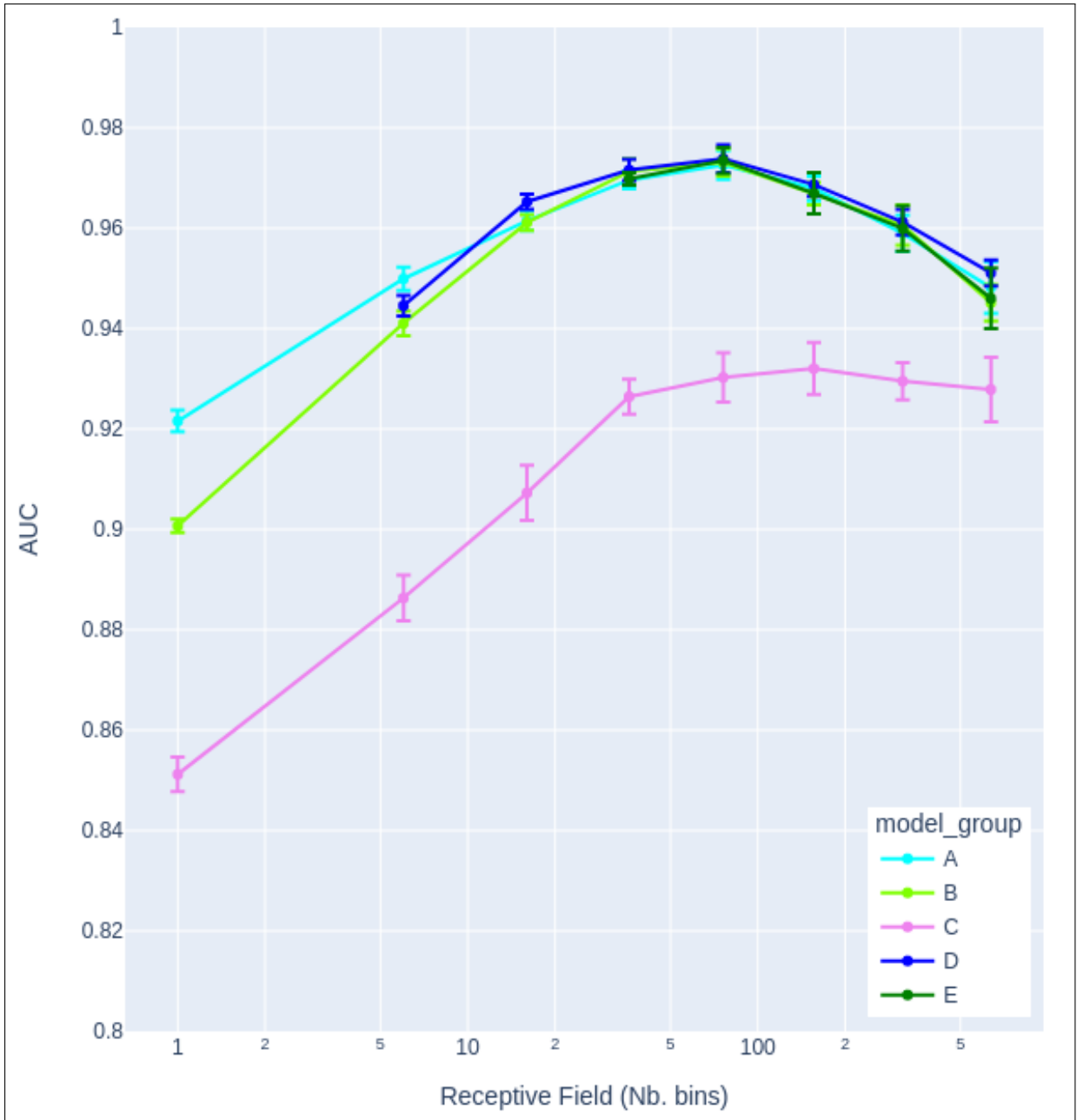


Figure 4: Macro AUC over all 20 classes for all SIMP-FU models plotted against MRF. Error bars are standard deviation over several training runs. Horizontal axis is logarithmic and goes from 1 to 636 time bins. See Table 4 to convert bins to seconds

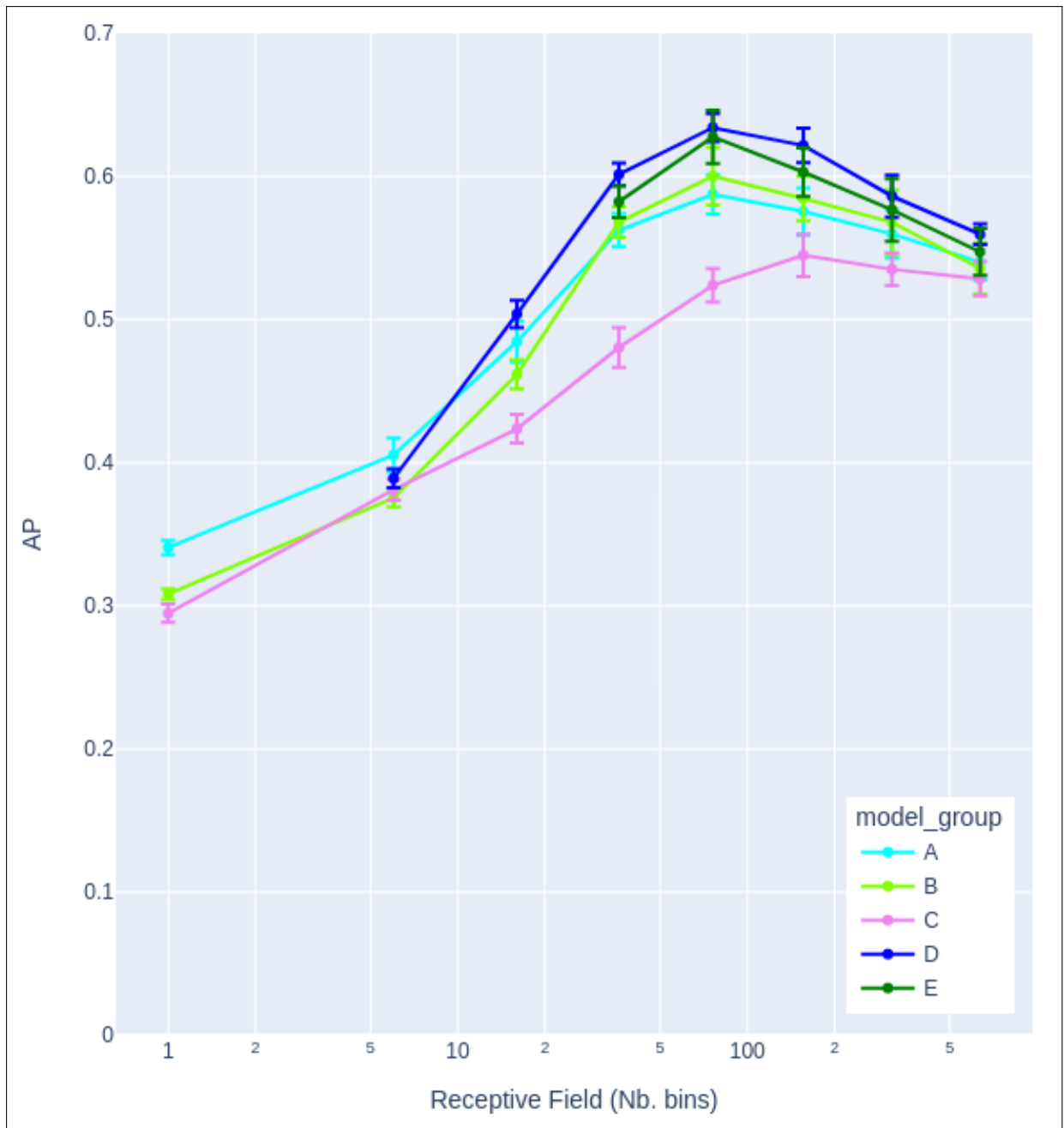


Figure 5: Macro AP over all 20 classes for all SIMP-FU models plotted against MRF. Error bars are standard deviation over several training runs. Horizontal axis is logarithmic and goes from 1 to 636 time bins. See Table 4 to convert bins to seconds

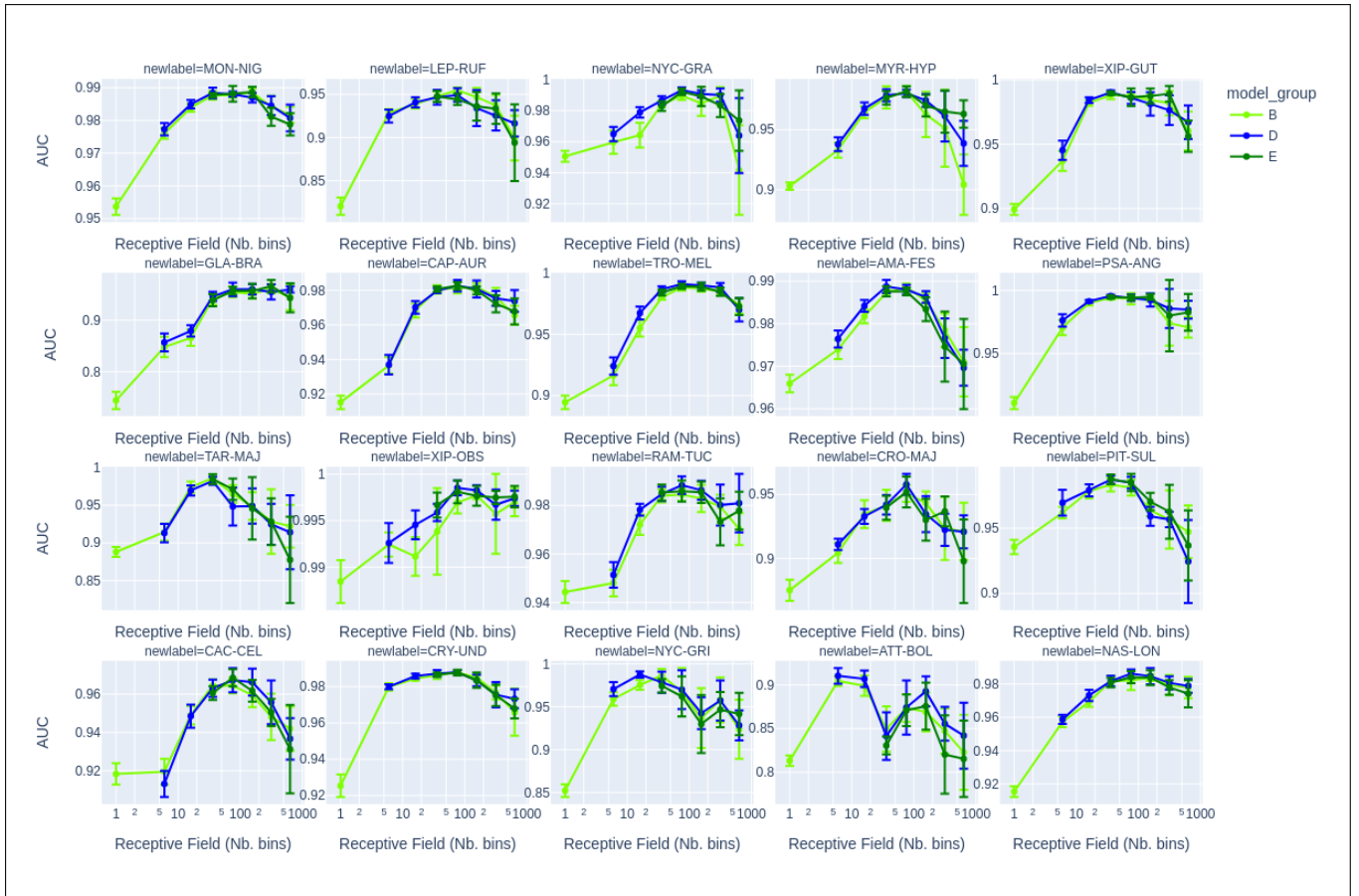


Figure 6: AUC plotted against MRF separately for each class. Vertical scale independent in each sub-plot to highlight the pattern within each class. For comparison of absolute performance see Figure 9

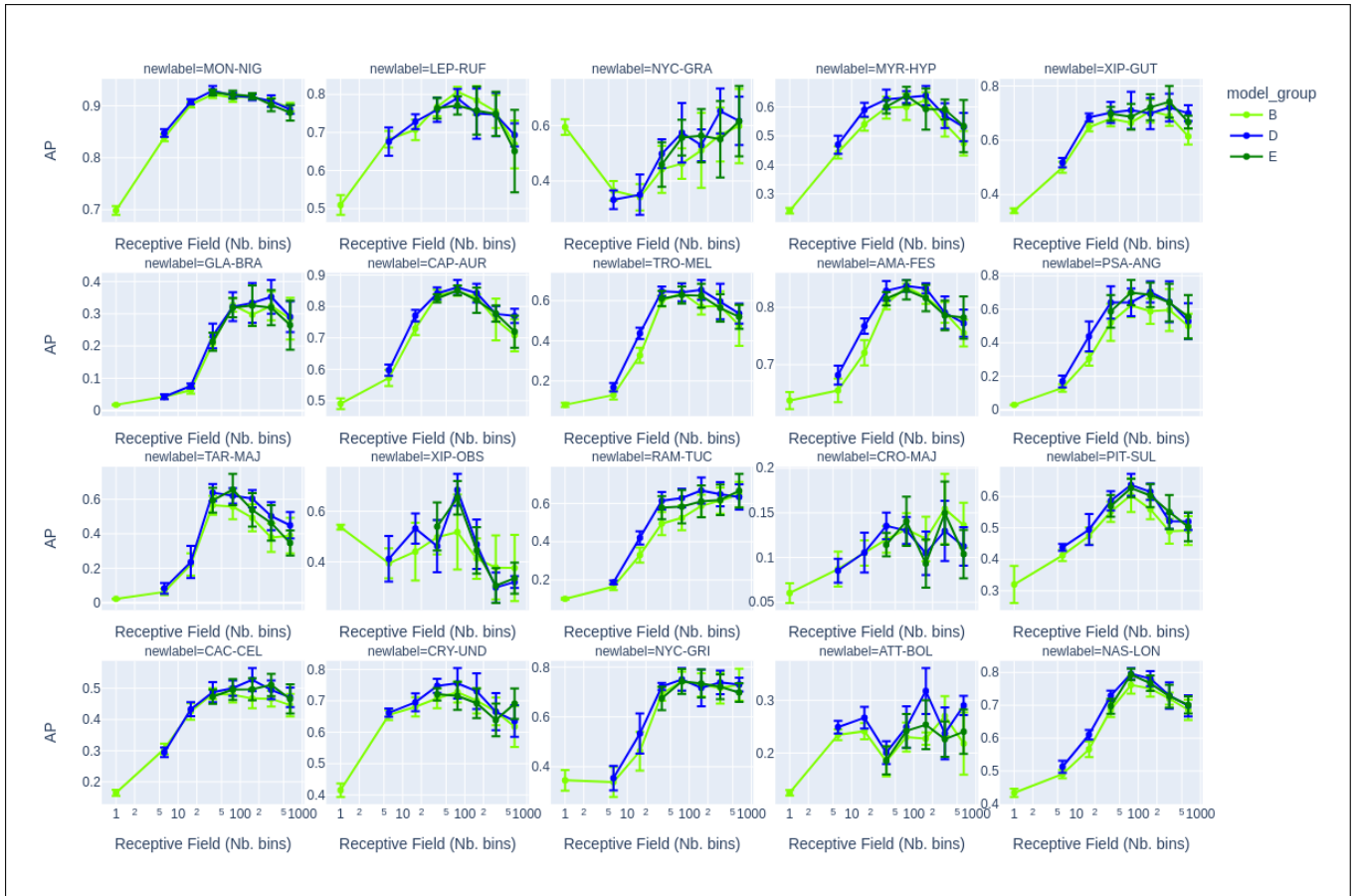
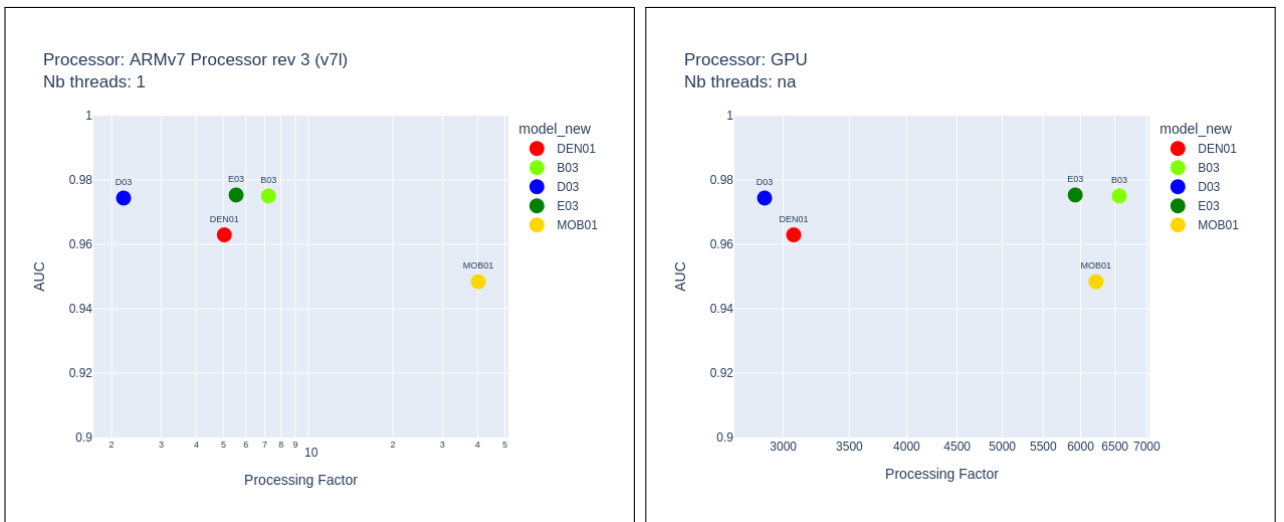


Figure 7: AP plotted against MRF separately for each class. Vertical scale independent in each sub-plot to highlight the pattern within each class. For comparison of absolute performance see Figure 9



(a) Compact low-cost device CPU

(b) High performance GPU processor

Figure 10: Classification strength (AUC) of subset of models plotted against processing factor from inference on a compact low-cost CPU with a single thread and batch size of 1 (a), and GPU processing with batch size of 32 (b).

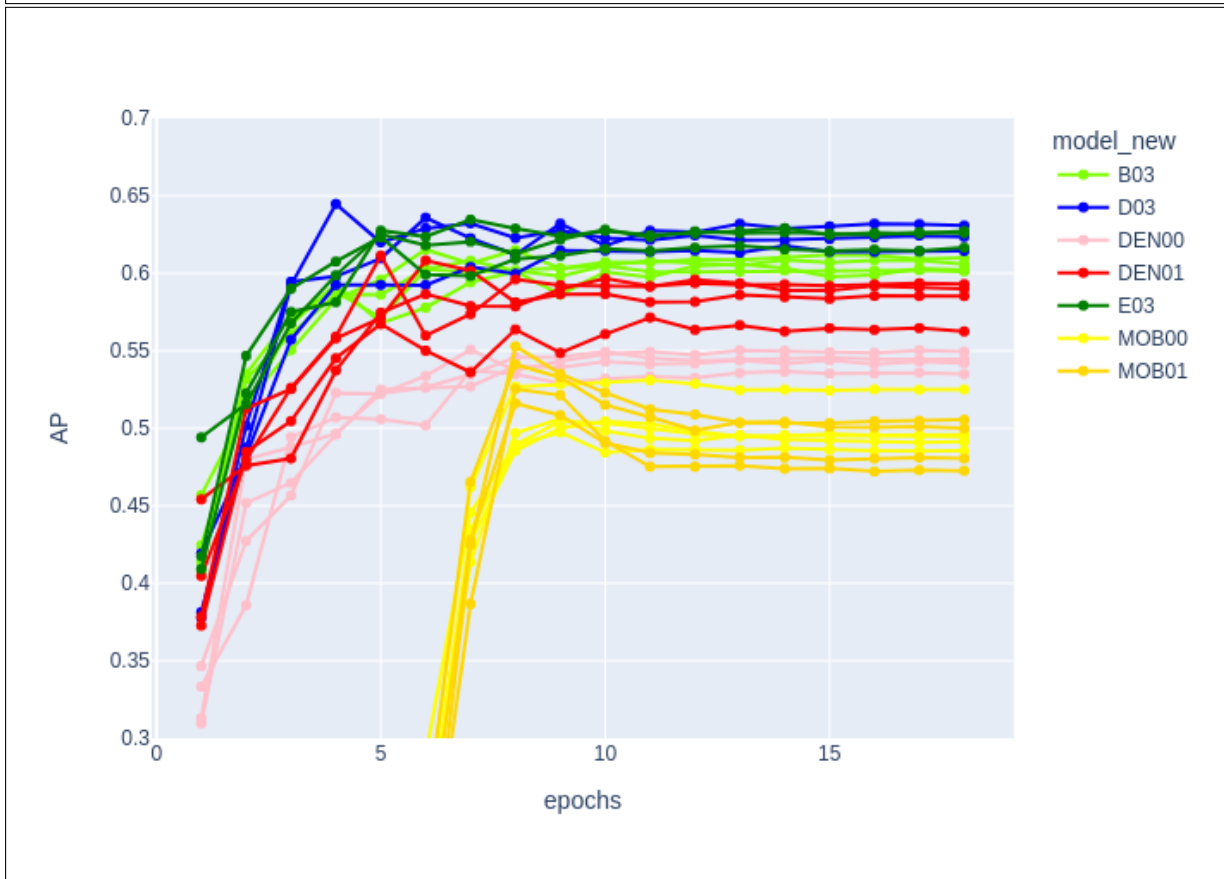
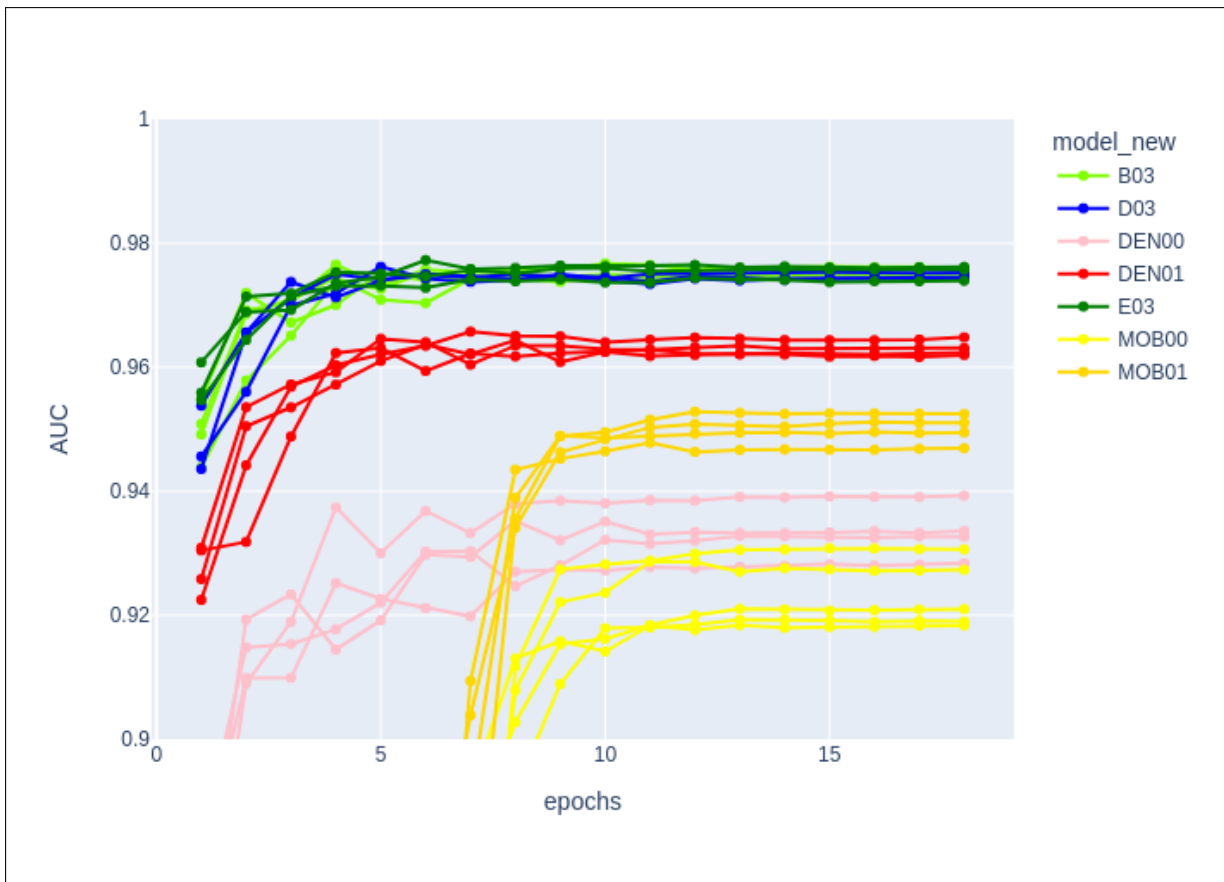


Figure 8: Performance vs epoch for the three best performing SIMP-FU models and the image CNN architectures

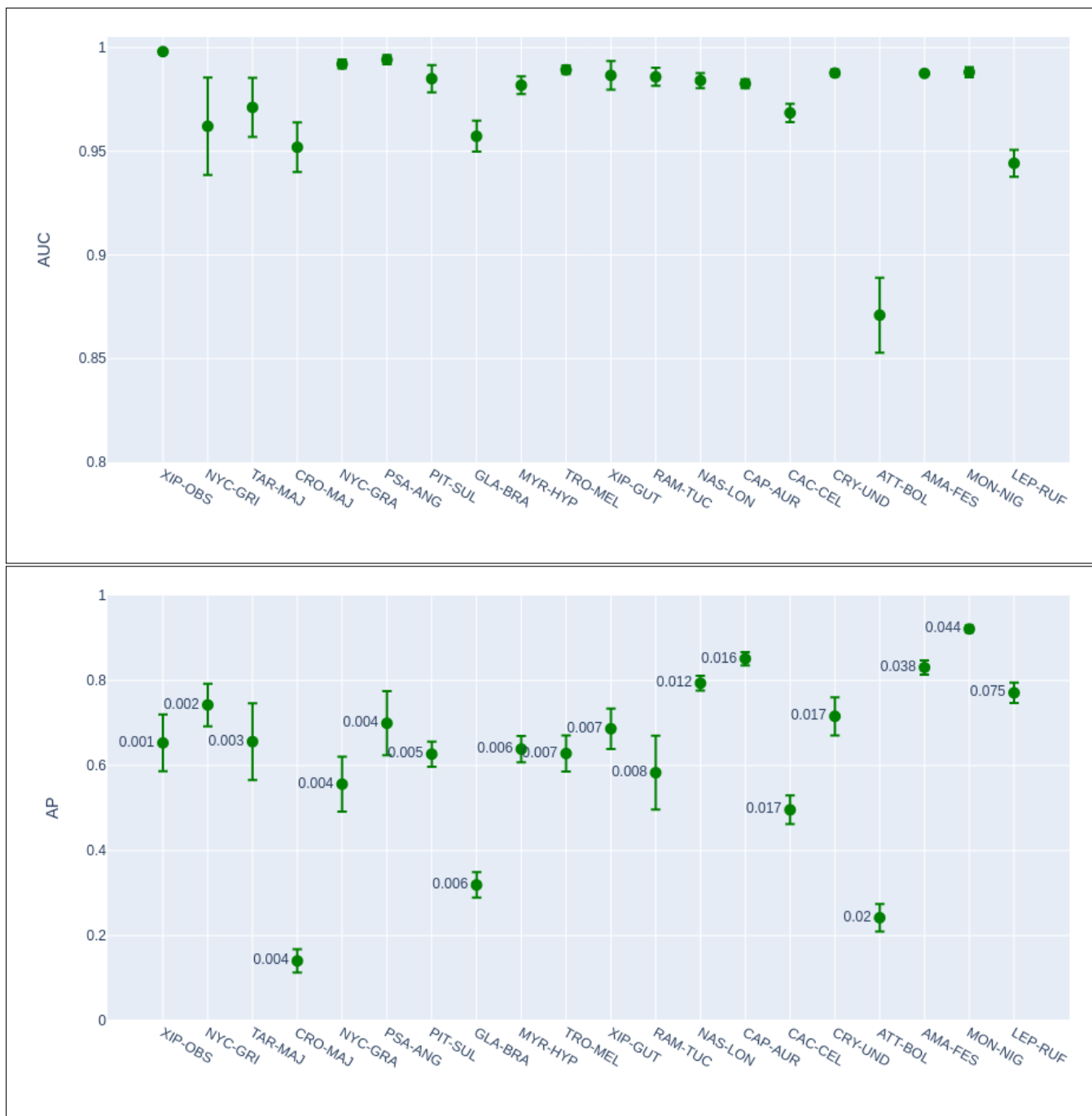


Figure 9: Per-class predictive performance of model E03. For AP the proportion of each class in the test set is annotated at each dot. Sound-types ordered left to right from lowest to highest proportion. Error bars are standard deviation over several training runs.

## 11 References

### References

- [1] Rory Gibb et al. “Emerging opportunities and challenges for passive acoustics in ecological assessment and monitoring”. In: *Methods in Ecology and Evolution* 10.2 (2019), pp. 169–185.
- [2] Robert Geirhos et al. “Shortcut learning in deep neural networks”. In: *Nature Machine Intelligence* 2.11 (2020), pp. 665–673.
- [3] Alexander D’Amour et al. *Underspecification Presents Challenges for Credibility in Modern Machine Learning*. 2020. arXiv: [2011.03395](https://arxiv.org/abs/2011.03395) [cs.LG].
- [4] Michael Bittle and Alec Duncan. “A review of current marine mammal detection and classification algorithms for use in automated passive acoustic monitoring”. In: *Proceedings of Acoustics*. Vol. 2013. Citeseer. 2013.
- [5] Marielle Malfante et al. “Automatic fish sounds classification”. In: *The Journal of the Acoustical Society of America* 143.5 (2018), pp. 2834–2846.
- [6] Nirosha Priyadarshani, Stephen Marsland, and Isabel Castro. “Automated bird-song recognition in complex acoustic environments: a review”. In: *Journal of Avian Biology* 49.5 (2018), jav–01447.
- [7] Jie Xie et al. “Frog call classification: a survey”. In: *Artificial Intelligence Review* 49.3 (2018), pp. 375–391.
- [8] Dan Stowell. *Computational bioacoustics with deep learning: a review and roadmap*. 2021. arXiv: [2112.06725](https://arxiv.org/abs/2112.06725) [cs.SD].
- [9] Jack LeBien et al. “A pipeline for identification of bird and frog species in tropical soundscape recordings using a convolutional neural network”. In: *Ecological Informatics* 59 (2020), p. 101113.
- [10] Yu Shiu et al. “Deep neural networks for automated detection of marine mammal species”. In: *Scientific reports* 10.1 (2020), pp. 1–12.
- [11] Thomas Grill and Jan Schlüter. “Two convolutional neural networks for bird detection in audio signals”. In: *2017 25th European Signal Processing Conference (EUSIPCO)*. IEEE. 2017, pp. 1764–1768.
- [12] Stefan Kahl et al. “Large-Scale Bird Sound Classification using Convolutional Neural Networks.” In: *CLEF (working notes)*. Vol. 1866. 2017.
- [13] Justin Salamon et al. “Fusing shallow and deep learning for bioacoustic bird species classification”. In: *2017 IEEE international conference on acoustics, speech and signal processing (ICASSP)*. IEEE. 2017, pp. 141–145.
- [14] Antoine Sevilla and Hervé Glotin. “Audio Bird Classification with Inception-v4 extended with Time and Time-Frequency Attention Mechanisms.” In: *CLEF (Working Notes)*. Vol. 1866. 2017.
- [15] Agnes Incze et al. “Bird sound recognition using a convolutional neural network”. In: *2018 IEEE 16th International Symposium on Intelligent Systems and Informatics (SISY)*. IEEE. 2018, pp. 000295–000300.

- [16] Mario Lasseck. “Audio-based Bird Species Identification with Deep Convolutional Neural Networks.” In: *CLEF (Working Notes)* 2125 (2018).
- [17] Songzuo Liu et al. “Classification of cetacean whistles based on convolutional neural network”. In: *2018 10th International Conference on Wireless Communications and Signal Processing (WCSP)*. IEEE. 2018, pp. 1–5.
- [18] Oisín Mac Aodha et al. “Bat detective—Deep learning tools for bat acoustic signal detection”. In: *PLoS computational biology* 14.3 (2018), e1005995.
- [19] Ivan Himawan et al. “Deep Learning Techniques for Koala Activity Detection.” In: *INTERSPEECH*. 2018, pp. 2107–2111.
- [20] Ali K Ibrahim et al. “Automatic classification of grouper species by their sounds using deep neural networks”. In: *The Journal of the Acoustical Society of America* 144.3 (2018), EL196–EL202.
- [21] André Araujo, Wade Norris, and Jack Sim. “Computing Receptive Fields of Convolutional Neural Networks”. In: *Distill* (2019). DOI: [10.23915/distill.00021](https://doi.org/10.23915/distill.00021).
- [22] Wenjie Luo et al. “Understanding the effective receptive field in deep convolutional neural networks”. In: *Proceedings of the 30th International Conference on Neural Information Processing Systems*. 2016, pp. 4905–4913.
- [23] Karen Simonyan and Andrew Zisserman. “Very Deep Convolutional Networks for Large-Scale Image Recognition”. In: (2015). arXiv: [1409.1556](https://arxiv.org/abs/1409.1556) [cs.CV].
- [24] Andrew G. Howard et al. *MobileNets: Efficient Convolutional Neural Networks for Mobile Vision Applications*. 2017. arXiv: [1704.04861](https://arxiv.org/abs/1704.04861) [cs.CV].
- [25] Mark Sandler et al. “Mobilenetv2: Inverted residuals and linear bottlenecks”. In: *Proceedings of the IEEE conference on computer vision and pattern recognition*. 2018, pp. 4510–4520.
- [26] Gao Huang et al. “Densely connected convolutional networks”. In: *Proceedings of the IEEE conference on computer vision and pattern recognition*. 2017, pp. 4700–4708.
- [27] Diederik P. Kingma and Jimmy Ba. *Adam: A Method for Stochastic Optimization*. 2017. arXiv: [1412.6980](https://arxiv.org/abs/1412.6980) [cs.LG].

## 12 Appendix

**External training set - detailed description** This data was downloaded from the xeno-canto repository ([www.xeno-canto.org](http://www.xeno-canto.org)). Geographic range was limited to Bolivia, Brazil, Ecuador, and Peru. The objective was to provide clear and unambiguous examples of the sound-types. We attempted to download at least 10 MP3 files of at least 600 seconds and took only files tagged with quality A or B whenever possible. Preference was given to shorter files but a file duration of at least 10 s was required. Files with a Non-Derivative (ND) license were excluded. All MP3 files were converted to WAV format and up-sampled to 48000 samples per second. After careful scrutiny of the metadata, we found that this data included 5 out of 547 files (212 out of 13302 seconds) that were recorded in the MSDR independently of the test set and did not overlap in time with the test set. These are highly selected recordings performed or selected by humans, sometimes with directional microphones. The sounds typically exhibit a high SNR. They are not representative of continuous recordings from the wild. While this data contains examples of target sounds, the background noise diversity is probably underrepresented.

sound type	Bolivia	Brazil	Ecuador	Peru	Qual. A	Qual. B	Qual. C	Tot nb files	Tot length (sec)
<i>Amazona festiva</i>	0	10	5	0	6	7	2	15	537
<i>Attila bolivianus</i>	2	17	0	5	12	12	0	24	641
<i>Cacicus cela</i>	1	12	18	4	24	11	0	35	639
<i>Capito aurovirens</i>	0	4	6	1	1	7	3	11	470
<i>Crotophaga major</i>	2	18	6	1	17	10	0	27	725
<i>Crypturellus undulatus</i>	0	19	4	3	19	7	0	26	666
<i>Glaucidium brasilianum</i>	2	23	4	1	20	10	0	30	663
<i>Leptotila rufaxilla</i>	2	14	6	4	16	10	0	26	682
<i>Monasa nigrifrons</i>	2	19	8	5	19	15	0	34	761
<i>Myrmelastes hyperythrus</i>	3	5	8	10	15	11	0	26	645
<i>Nasica longirostris</i>	1	11	10	2	14	10	0	24	606
<i>Nyctibius grandis</i>	2	9	2	3	3	13	0	16	713
<i>Nyctibius griseus</i>	1	15	6	0	13	9	0	22	643
<i>Pitangus sulphuratus</i>	3	22	11	2	20	18	0	38	663
<i>Psarocolius angustifrons</i>	4	7	26	4	28	13	0	41	731
<i>Ramphastos tucanus</i>	0	17	9	5	23	0	8	31	847
<i>Taraba major</i>	5	21	14	5	26	19	0	45	847
<i>Trogon melanurus</i>	3	8	7	0	15	3	0	18	627
<i>Xiphorhynchus guttatus</i>	4	24	7	5	22	18	0	40	722
<i>Xiphorhynchus obsoletus</i>	4	7	6	1	10	7	1	18	474
All	41	282	163	61	323	210	14	547	13302

Table 6: Details on files downloaded from xeno-canto that were included into the training set.

Species	Description	Duration Group	Additional Metric	Train	Train	Train	Train	Test	Test
				Period 2	XC	All	Up-sampled	Period 1	Period 1
				N	N	N	N	N	Prop
— Fixed duration			Approx duration	10242	1099	11341	14670	5635	
<i>Attila bolivianus</i>	Song	FD1	3+ sec	1	31	32	224	115	0.02
<i>Taraba major</i>	Song	FD1	3+ sec	0	40	40	200	15	0.003
<i>Nyctibius griseus</i>	Song	FD1	3+ sec	1	38	39	234	10	0.002
<i>Xiphorhynchus guttatus</i>	Song	FD1	3+ sec	9	32	41	205	40	0.007
<i>Myrmelastes hyperythrus</i>	Song	FD2	1 – 3 sec	3	37	40	224	33	0.006
<i>Xiphorhynchus obsoletus</i>	Song	FD2	1 – 3 sec	0	33	33	231	8	0.001
<i>Crypturellus undulatus</i>	Song	FD2	1 – 3 sec	73	43	116	251	96	0.017
<i>Nasica longirostris</i>	Song	FD3	0.5 – 1 sec	36	28	64	297	65	0.012
<i>Nyctibius grandis</i>	Song	FD3	0.5 – 1 sec	8	52	60	243	22	0.004
<i>Psarocolius angustifrons</i>	Song	FD3	0.5 – 1 sec	10	28	38	228	24	0.004
<i>Pitangus sulphuratus</i>	Call	FD3	0.5 – 1 sec	26	47	73	222	26	0.005
<i>Leptotila rufaxila</i>	Song	FD3	0.5 – 1 sec	8	54	62	269	420	0.075
— Variable duration			Repet. interval						
<i>Ramphastos tucanus</i>	Song	VD1	0.5 sec	26	68	94	323	44	0.008
<i>Trogon melanurus</i>	Song	VD1	0.7 sec	50	43	93	331	38	0.007
<i>Capito aurovirens</i>	Song	VD1	0.5 sec	283	30	313	449	90	0.016
<i>Glaucidium brasilianum</i>	Song	VD1	0.3 sec	44	43	87	265	33	0.006
<i>Amazona festiva</i>	Call	VD2	irregular	54	45	99	305	213	0.038
<i>Cacicus cela</i>	Call	VD2	irregular	94	17	111	229	95	0.017
<i>Crotophaga major</i>	Call	VD2	irregular	8	19	27	216	22	0.004
<i>Monasa nigrifrons</i>	Song	VD2	irregular	91	44	135	300	250	0.044

Table 7: Details on training and test data.

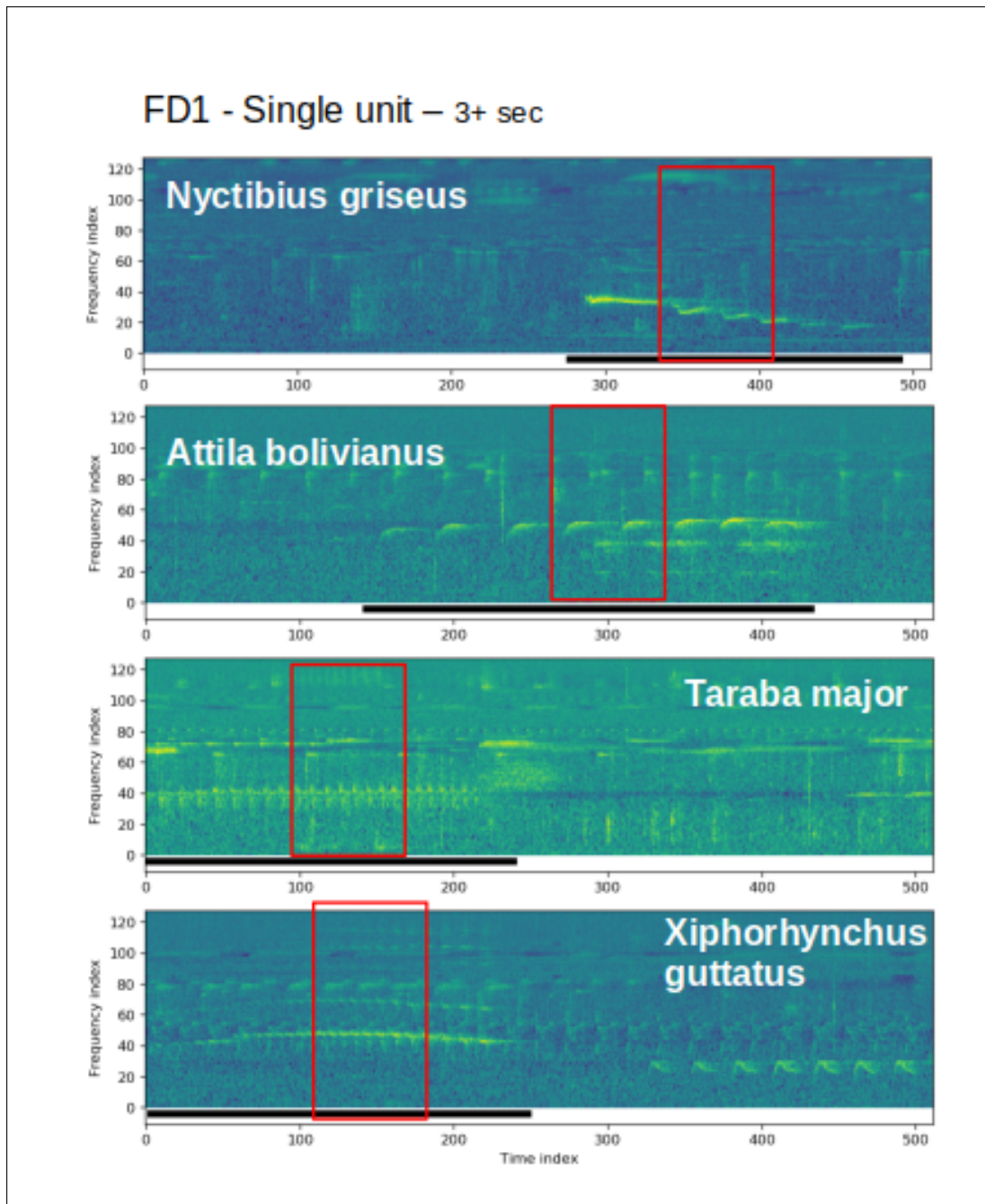


Figure 11: Spectrograms used as CNN input. Sound-types that were equal or longer than 3 seconds. Time-indexed labels used as target during training shown as black bars at the bottom of each spectrogram. Manually selected Regions of 1.5 seconds shown as red boxes to allow visual comparison with the time scale of acoustic patterns.

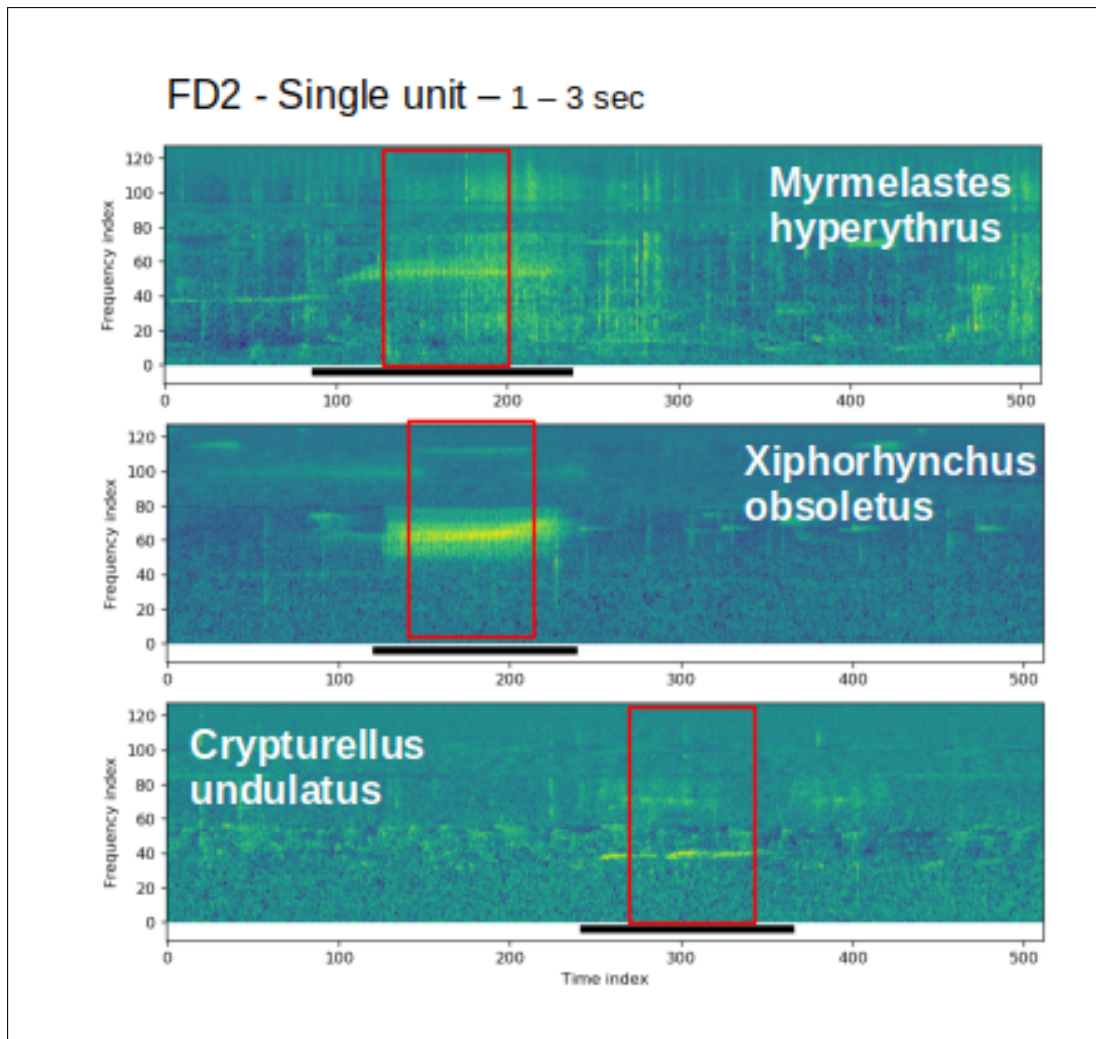


Figure 12: Spectrograms used as CNN input. Sound-types that were between 1 and 3 seconds.

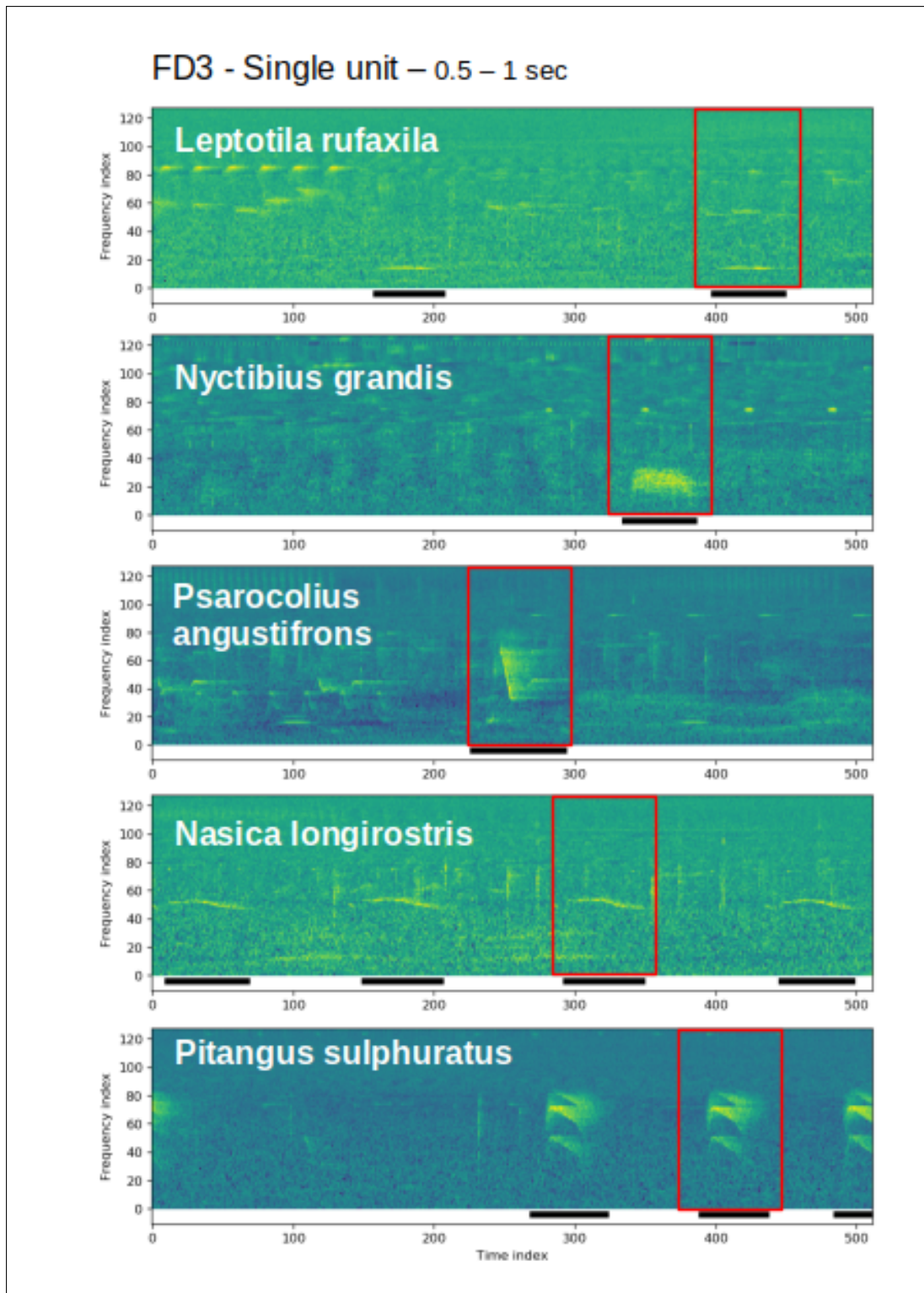


Figure 13: Spectrograms used as CNN input. Sound-types that were between 0.5 and 1 seconds.

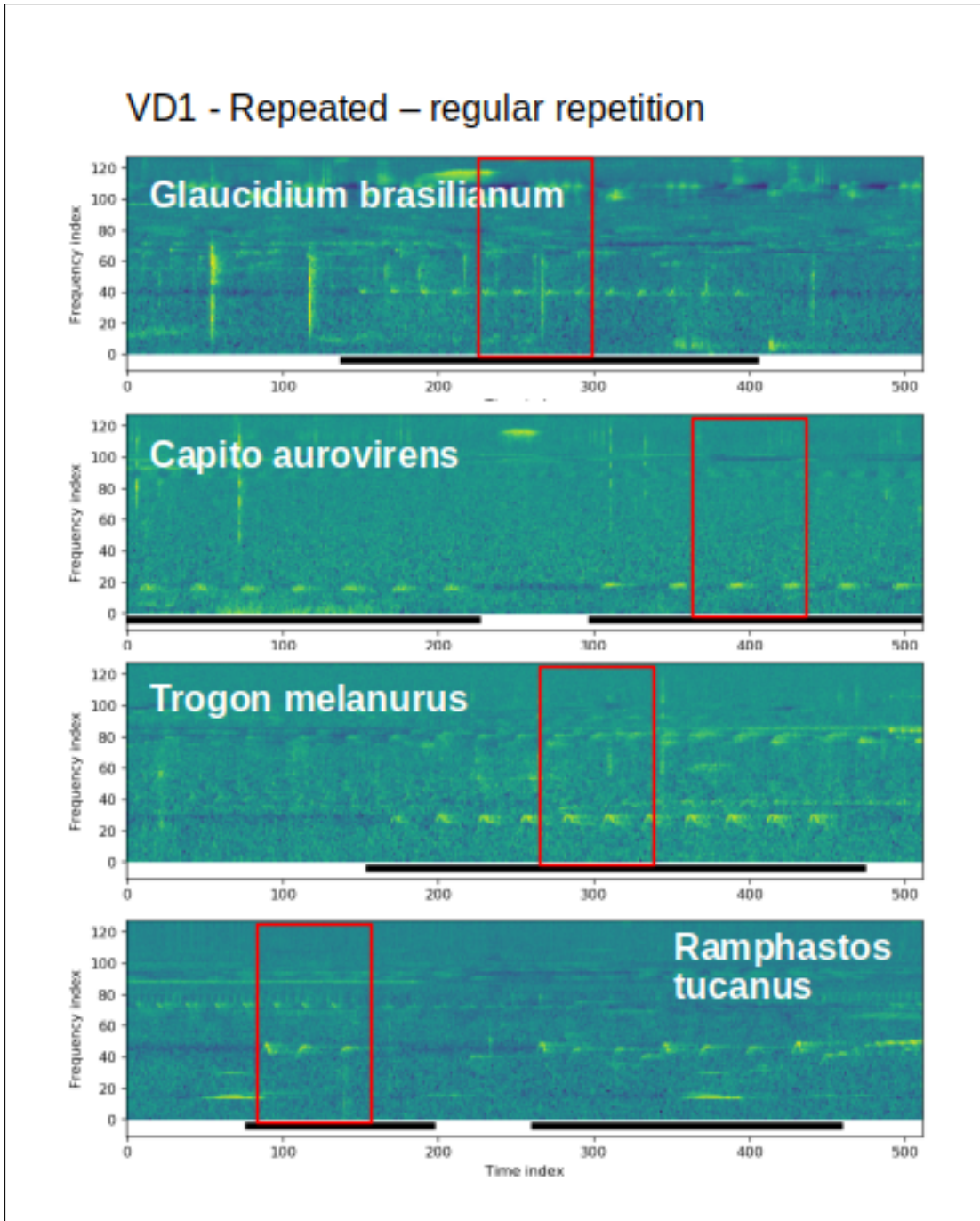


Figure 14: Spectrograms used as CNN input. Sound-types with regular repetition pattern

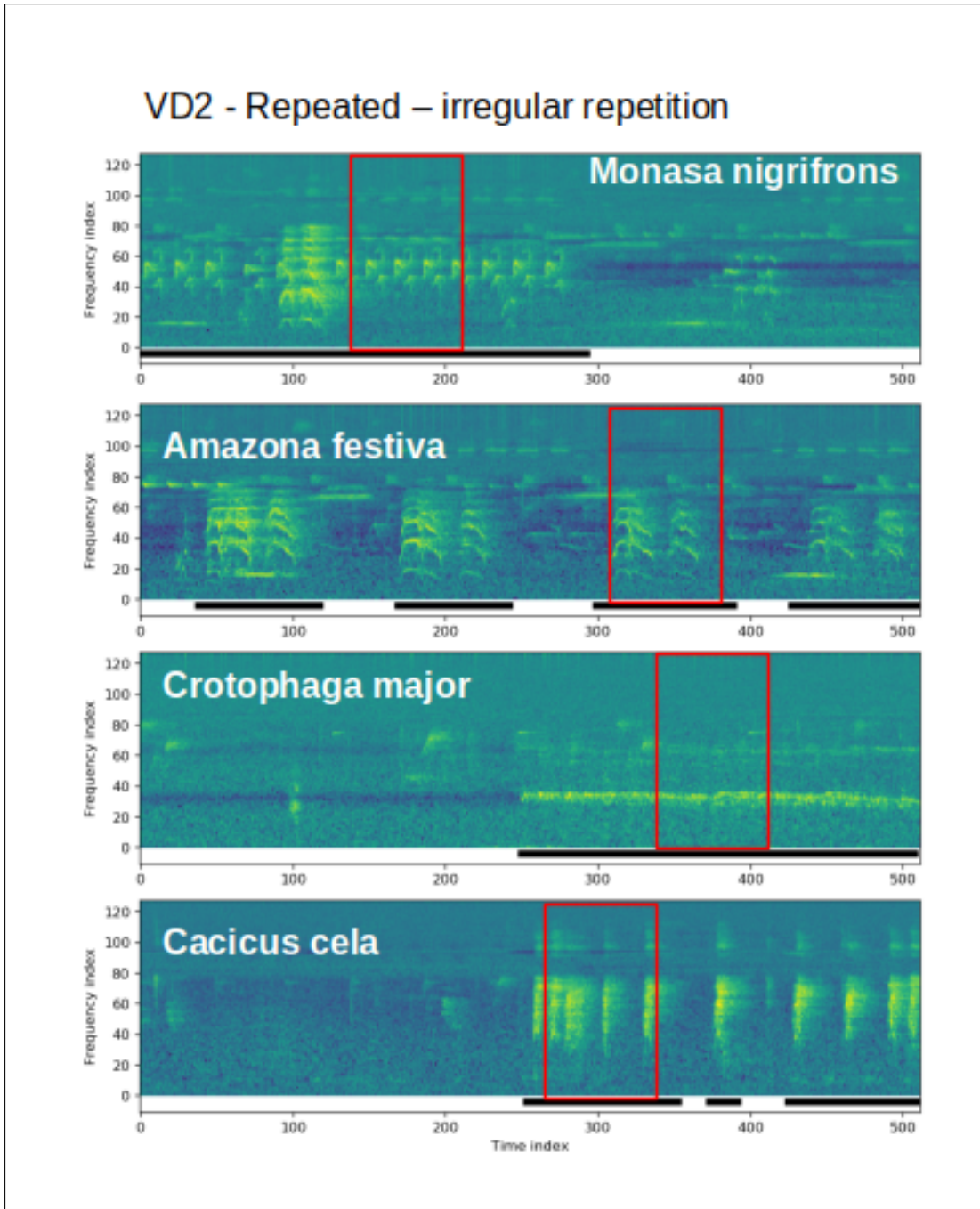
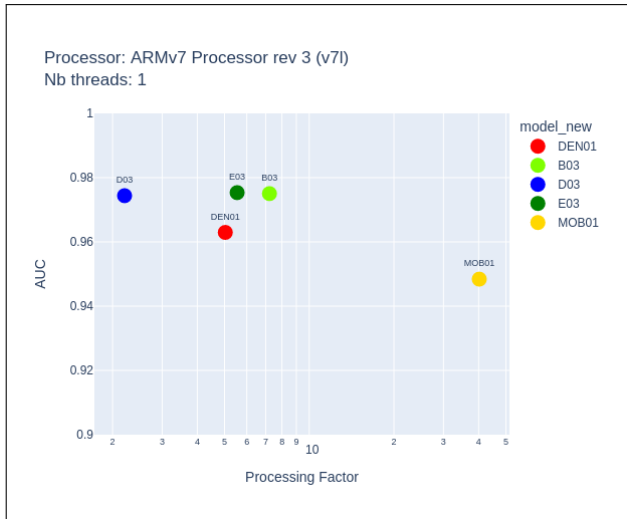
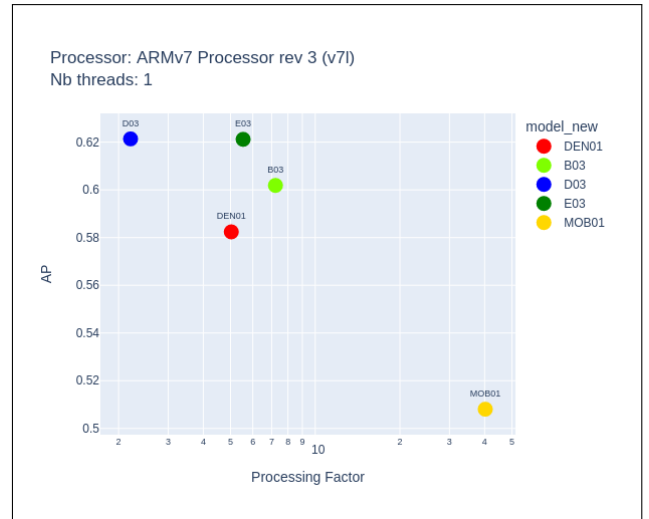


Figure 15: Spectrograms used as CNN input. Sound-types with non-regular repetition pattern

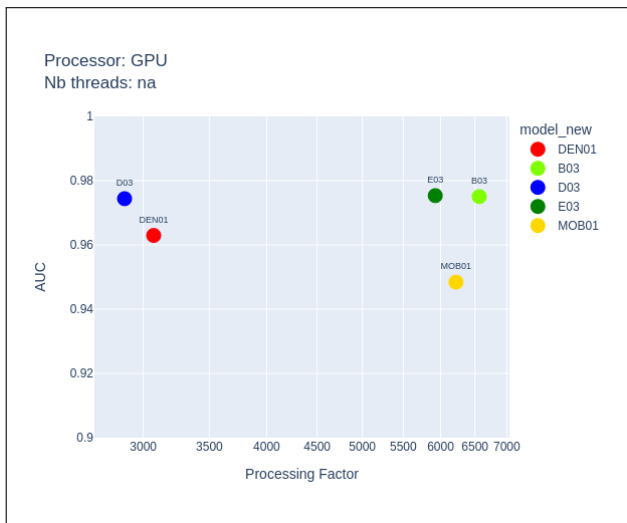


(a) AUC

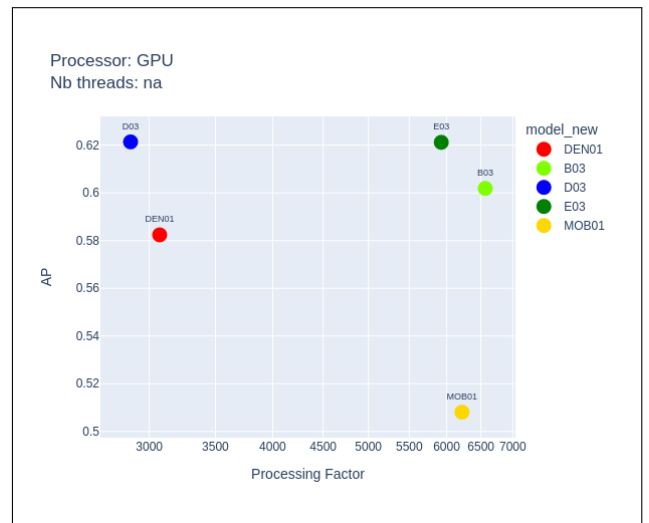


(b) AP

Figure 16: Predictive performance of subset of high-performing models plotted against processing factor from inference on a low-performance CPU with a single thread and batch size of 1



(a) AUC



(b) AP

Figure 17: Same as Figure 12 but inference on GPU with batch size of 32